A review of acoustic power transfer for bio-medical implants

2016 Smart Mater. Struct. 25 123001

(http://iopscience.iop.org/0964-1726/25/12/123001)

IOP Publishing Smart Materials and Structures
Smart Mater. Struct. **25** (2016) 123001 (23pp) doi:10.1088/0964-1726/25/12/123001

Topical Review

A review of acoustic power transfer for bio-medical implants

Hamid Basaeri, David B Christensen and Shad Roundy

Department of Mechanical Engineering, University of Utah, Salt Lake City, UT, USA

E-mail: h.basaeri@utah.edu

Received 18 July 2016, revised 12 September 2016
Accepted for publication 3 October 2016
Published 11 November 2016

Abstract

Bio-implantable devices have been used to perform therapeutic functions such as drug delivery or diagnostic monitoring of physiological parameters. Proper operation of these devices depends on the continuous reliable supply of power. A battery, which is the conventional method to supply energy, is problematic in many of these devices as it limits the lifetime of the implant or dominates the size. In order to power implantable devices, power transfer techniques have been implemented as an attractive alternative to batteries and have received significant research interest in recent years. Acoustic waves are increasingly being investigated as a method for delivering power through human skin and the human body. Acoustic power transfer (APT) has some advantages over other powering techniques such as inductive power transfer and mid range RF power transmission. These advantages include lower absorption in tissue, shorter wavelength enabling smaller transducers, and higher power intensity threshold for safe operation. This paper will cover the basic physics and modeling of APT and will review the current state of acoustic (or ultrasonic) power transfer for biomedical implants. As the sensing and computational elements for biomedical implants are becoming very small, we devote particular attention to the scaling of acoustic and alternative power transfer techniques. Finally, we present current issues and challenges related to the implementation of this technique for powering implantable devices.

Keywords: implantable devices, energy harvesting, ultrasonic transducer, wireless power transfer

(Some figures may appear in colour only in the online journal)

1. Introduction

Bio-implantable or implantable medical devices (IMDs) are devices designed for monitoring biological parameters, drug delivery, or improving the function of certain organs in the human body. The expanded use of IMDs for monitoring patient health will be an essential medical instrument in the near future. Patients with serious diseases such as bradycardia, fibrillation, and diabetes, to name just a few, may need these devices for their survival [1]. The existing interaction between medicine and technology allows for the development of new implantable devices to detect or monitor diseases inside the human body [2–4]. For instance, an implantable glucose sensor permits diabetics to obtain real-time, accurate glucose readings without pricking their finger [5]. Other IMDs, such as those to measure blood pressure and implanted microelectrodes to monitor cerebral or intramuscular electromyographic (EMG) signals, are explained in [6–8].

An implantable device needs a reliable supply of power for operation. Batteries, the traditional method of supplying power to implants, eventually require replacement which typically requires invasive surgery. Although they are a convenient and reliable source of energy with relatively high energy density, they are not the best candidate to power small implantable devices due to their limited lifetime. If the implant is large, and a large battery can be included, the lifetime may be many years [9, 10]. However, typically implants should be as small as possible to reduce trauma to the patient, and miniaturization of power sources has not kept pace with the shrinking size of the sensing and computational

elements. Subsequently, onboard power sources such as a battery can dominate the size of implants and be a limiting factor for miniaturization [11, 12]. This fact has led to a rich field of research on alternative methods to power implants.

For example, bio-medical devices can be powered by implantable fuel cell systems that are capable of converting endogenous substances and oxygen into electricity using a spatially separated electrochemical reaction. Glucose is one of the most common fuels due to its ubiquitous availability in the human body. Fuel cells enabled by enzymatic, microbial, and abiotically catalyzed reactions have all been proposed and demonstrated [13]. The state-of-the-art in abiotically catalyzed glucose fuel cells is fully reviewed by Kerzenmacher *et al* [14]. Based on their literature survey, abiotically catalyzed glucose fuel cells can generate power densities between 2.5 and 8 μW cm^{-2} for no longer than 100 days in *in vitro* experiments. Although this is a promising direction for future research and development, current state of the art does not support powering long term bio-implantable devices.

Vibrational or kinetic energy harvesting has also been proposed as a technique to power implantable devices. Vibrational energy harvesting systems harvest the energy of human motion in order to power a device. Generally speaking, vibration intensity available inside the body is usually very low [15], and therefore, cannot be considered as an appropriate method to power implantable devices. However, in certain specific applications, sufficient kinetic energy is available to harvest. These harvesters may use different methods to convert energy from the motion of the human body to electrical energy such as electromagnetic, electrostatic, and piezoelectric conversion. An electromagnetic generator for diaphragm muscle movement developed in [16] is capable of producing up to 1 mW of power, but at an approximate volume of 16 cm^3 the power density is only 0.062 mW cm^{-3}. Chen *et al* [17] developed a device to be embedded in orthopedic implants which produces 1.2 mW in a volume of 0.45 cm^3. Although the power density of this device, 2.66 mW cm^{-3}, is enough for powering implantable devices, it is feasible only for knee implants since this power density can be achieved only in the presence of a 900 N force. Additionally, pacemakers can be powered from heartbeat vibrations. Karami and Inman have investigated the use of vibration energy harvesters for charging the batteries of pace makers as their power requirement is low (around 1 μW) [18, 19]. Their device can generate 8 μW of power from heartbeat oscillations. For a more detailed comparison and discussion of vibrational energy harvesting for implantable medical devices, we refer the reader to Hanan *et al* [20], Cadei *et al* [21], and Romero *et al* [22]. Other alternative energy harvesting methods such as optics [23], and thermal gradients [24] have also been implemented to power implantable devices, however, as temperature differentials and light are very scarce inside the body they are usually not very effective.

Given the limitations of batteries, and the challenge with harvesting existing energy within the body, there has been an increasing research effort on methods to wirelessly transfer power to medical implants [12, 20, 25–27]. These methods include power transfer by mid to far field radio frequency (RF) radiation, inductive power transfer (IPT), and acoustic (or ultrasound) power transfer (APT). Each method has some benefits. However, as the size of the implant shrinks and the depth grows, it has been shown that ultrasonic power transfer can be fundamentally more efficient than IPT [28, 29]. The goal of this paper is to review the state-of-the-art in transferring power to bio-implantable devices using APT. In so doing, we will briefly review power transfer by both coupled electromagnetic coils and mid to far field RF methods for comparison. However, the bulk of the review will specifically cover APT. The remainder of this paper is organized as follows: we first compare RF, coupled inductive coils, and acoustic techniques. Second, we will cover the fundamentals of APT including common modeling techniques. We will review published studies and acoustic power implementations along with their transducer designs. Finally, we draw some conclusions about profitable directions for future research.

2. Comparison of power transfer methods for medical devices

Radio waves cover the range of 3 kHz–300 GHz of the electromagnetic spectrum. The use of a set of transmitting and receiving antennas operating in the RF range allows for the transmission of power. For the purposes of this paper, we categorize electromagnetic transmission as either IPT if the coupling is in the near field, or RF if the coupling is in the mid field (i.e. transition region) or far field. We note that this differentiation is not universal in the literature, and often systems that exhibit near field coupling are referred to as RF. Nevertheless, in this paper, we will follow this classification. Far field RF transmission is omnidirectional and thus suffers from low efficiency. One of the major drawbacks of this method is that it loses its strength as it spreads further away from the source, and therefore, a very small amount of power is available to be harvested. Furthermore, this kind of radiation can cause potential risks to humans, thus the generated power should be applied only to low power applications (mW and μW) since the output power is restricted by government regulations [12]. As an example, Shih *et al* presented a pressure/temperature sensing device for continuous intraocular pressure monitoring with a single turn 10 mm diameter loop antenna to generate 2.3 μW of power operating at 2.4 GHz [30]. Poon *et al* proposed a mid field RF powering technique to increase the gain of the transmitted power signal and to avoid spreading. However, it does not overcome the issue with high attenuation in tissue [31, 32]. Microwaves, a sub-section of radio waves in the range of 3–300 GHz, can transfer power over long distances, however, they are not widely used since they are not safe when the RF exposure density is high. A schematic of a RF power transfer system is depicted in figure 1(a).

Inductive power transfer systems usually consist of two coupled coils which have the same inductance as shown in figure 1(b). The transmitter coil is placed outside of the body whereas the receiver coil is integrated with the implanted

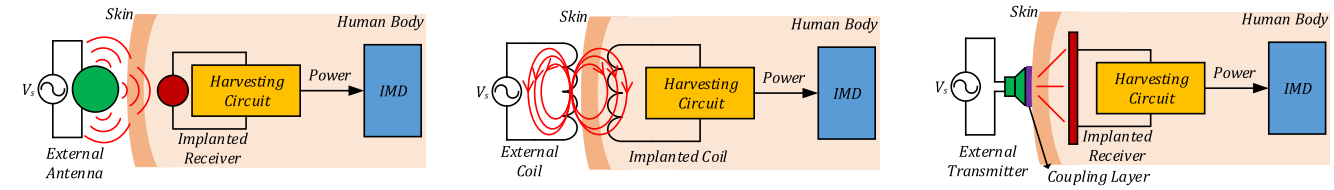

a) Radio frequency b) Inductive coupling c) Acoustic

Figure 1. Different power transfer methods for powering IMDs.

device inside the body. When a sinusoidal current is placed on the transmitter coil, a voltage is induced in the receiver coil as a result of electromagnetic induction [25]. The generated voltage is conditioned and then fed to the IMD. The highest power and efficiency is achieved when both coils are tuned to their resonance frequency [29]. There are several factors which can affect the efficiency of the wireless power transfer including resonance frequency (or operating frequency) and coupling between the transmitter and the receiver coils which itself can be affected by distance and alignment. The inefficiency of IPT in a large space is discussed in [33], and it is stated that this kind of energy transfer is not practical for large distances because as the distance between transmitter and receiver coils compared to the coils' diameters increases, the coupling goes down leading to high conduction losses due to excessive reactive current. The literature is full of examples of IPT and RF powered sensors, including biomedical implants. A full review of this work is not possible here. Suffice it say that these methods clearly work, but suffer at small sizes and deep implant depths because the efficiency becomes very poor.

Acoustic energy is emitted from diverse types of mechanical waves which are capable of penetrating through gases, liquids and solids [34]. It can be harvested from the ambient environment or transferred wirelessly to a receiver as shown in figure 1(c). Typically, the acoustic wave, which is usually at ultrasound frequencies, is generated by a piezoelectric transducer that is in contact with the skin. The pressure wave transmits through the tissue and induces a voltage on a receiver structure which is also typically a piezoelectric device [35]. In the context of implanted devices, acoustic waves have some significant advantages over electromagnetic waves: they have shorter wavelengths which result in smaller sized receiving transducers, and they exhibit lower attenuation in human tissue which results in deeper penetration. Furthermore, some focusing techniques such as the one presented in [36] can be implemented on these devices due to the fact that their wavelengths are in the range of mm. These waves are safe to use in the human body at diagnostic intensities, and they are not susceptible to electromagnetic interference [37]. The transducers can also be designed in a compact size, which is an important feature for implantable devices. Acoustic waves are suitable for propagation within the predominantly liquid environment inside the human torso, and cause minimal tissue heating when operating at lower frequencies. There are some applications in which the implant incorporates electrodes and wiring to these electrodes. Electromagnetic power transfer can cause unwanted voltages on these wires which may result in unintentional excitation whereas ultrasonic power transfer does not suffer from this problem. A more detailed discussion of the devices reported in the literature and the current state of the art will be presented in section 5.

Each of these power transfer approaches for implantable devices has its own advantages and weaknesses. Inductive coupling works in the near field, and the transferred power is reduced according to the cube of the reciprocal of the charging distance [38]. On the other hand, RF radiation works in the far field at a longer distance relative to the size of the antenna. The power in far field systems reduces according to the square of the reciprocal of the charging distance [38]. Additionally, there is no need for the transmitting and receiving antennas to be coupled for RF. However, for inductive coupling, the transmitting and receiving coils should be coupled [39]. Although inductively coupled power transfer systems can be implemented in a simple way, they need more accurate alignment than RF systems. Moreover, they have a shorter effective powering distance which makes using them difficult in implantable devices [40]. Furthermore, electromagnetic waves can generate excessive tissue heating, affecting the immune system, calcium metabolism and DNA synthesis [41, 42]. The efficiency of inductive and RF power transfer drops dramatically as the size decreases [43, 44] due to the relatively large wavelength of electromagnetic waves and the increased attenuation at high frequencies. For instance, a single turn 10 mm diameter loop antenna implanted at 15 mm depth has been shown to generate 2.3 μW [30]. However, the same amount of power at the same depth could be generated by an acoustic generator with a diameter of 1 mm or less [45, 46]. Overall, the research literature indicates that obtaining more power with smaller devices can be achieved by the use of APT.

Several devices utilizing differing power sources are compared in table 1 in terms of their frequency, power and size. As shown in figure 2, the operating frequency of RF devices is generally higher than inductive coupling and acoustic devices. Most RF and inductive coupling devices are tested in air while APT is usually analyzed in water or tissue. Figure 3 gives the depth of the implanted device in the body versus the receiver size for different devices in table 1 and shows that the implant depth for APT devices is typically higher compared to RF and IPT for the same size device. Figure 4 plots the output power intensity at the receiver face for these devices against the receiver size, and shows that typically higher power density is achieved using acoustics compared to RF and IPT devices with almost the same size.

Table 1. Comparison of several implantable devices with different powering mechanisms.

Method	Article		Efficiency (%)	Frequency (MHz)	Output power (mW)	Receiver area (cm^2)	Power intensity ($mW\ cm^{-2}$)	Depth (mm)	Medium
	Author	Year/Ref							
Radio frequency (RF)	O'Driscoll	2009/[49]		1000	0.14	0.04	3.5	15	
	Poon	2010/[47]	0.2	1000	0.005	0.04	0.125	40	
	Shih	2011/[30]	1.73	2400	2.3×10^{-3}	0.78	0.0029	15	Tissue
	Ho	2014/[31]	0.04	1600	0.2	0.04	5	50	
Inductive coupling (IPT)	Jow	2007/[50]	85.5	5		4		10	Air
	Kilinc	2010/[51]	66.7	13.56		4		30	Air
	Kiani	2010/[52]	1.02	13.56	11.2	1	11.2	20	Air
	Kiani	2011/[53]	4.82	13.56	27	1.2	22.5	7	Air
	Silay	2011/[54]	54.98	8	10	1	10	10	Air
	Liu	2013/[55]		13.56	0.95	3	0.317	24	Pig skin
Acoustic (APT)	Arra	2007/[56]	25	0.84	62.5	4.9	12.73	100	Water
	Larson	2011/[57]	0.022	1	0.51	0.01	51	120	Rat hind limb
	Sanni	2012/[58]	1	0.2	8	0.78	10.26	70	Water
	Mazzilli	2014/[59]	1.6	1	28	0.3	93.33	105	Water

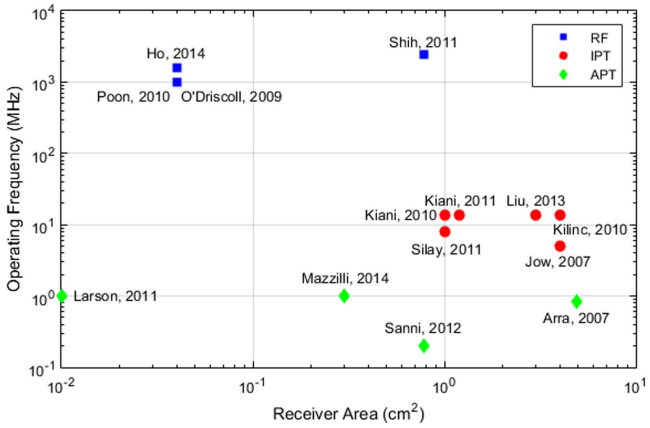

Figure 2. Operating frequency of reported devices versus receiver area.

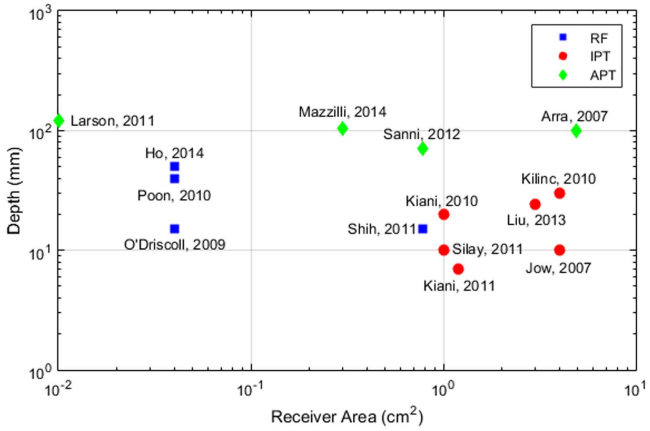

Figure 3. Implanted depth of reported devices versus receiver area.

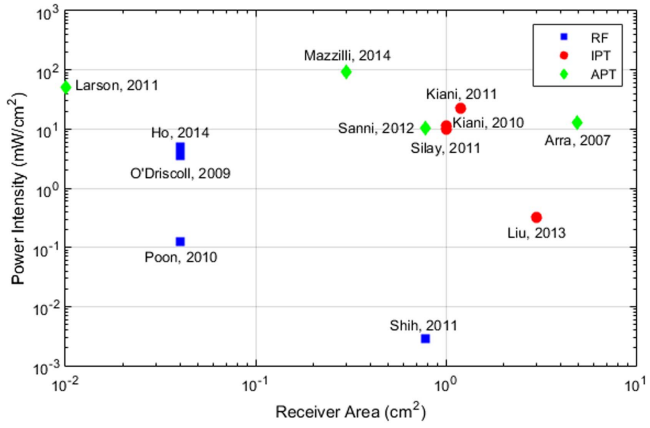

Figure 4. Output power intensity of reported devices versus receiver area.

For example, Poon *et al* [47] studied the optimal frequency for RF power transfer in tissue for a 4 mm^2 receiver. Their studies indicate an optimal efficiency of 0.2% at an implant depth of 4 cm. The resulting power generation would be 5 μW or 1.25 μW mm^{-2}. Note that if a 1 mm^2 receiver were used, the power generation may be even lower than 1.25 μW as the scaling is not necessarily linear. Alternatively, using the power transmission models developed by Denisov *et al* [29], an acoustic power receiver of the same size at the same implant depth has an optimal efficiency of 2% (compared to 0.2% for RF). Given the increased efficiency, and the fact that the food and drug administration (FDA) limits for power transmission into tissue are higher for ultrasound (7200 μW mm^{-2}) than for RF radiation [48], the resulting optimal power density for acoustics is 144 μW mm^{-2}. With a 4 mm^2 receiver, 576 μW could be transferred. It should be noted that these FDA limits are for imaging or high intensity focused ultrasound devices since there is no specific limitation for ultrasound power transfer operating in continuous wave (CW) mode. Moreover, the safety limitations are not the same for all organs in the body. The 7200 μW mm^{-2} limitation is intended for peripheral vessels, however, there are some other organs such as cardiac, abdominal, and ophthalmic organs having much lower limitations [44]. Operating frequency is another important factor affecting the regulation limits. The dependency of safety limits to the operating frequency will be covered in the frequency selection section. Thus, at these very small sizes and large implant depths, an acoustically powered sensor would have roughly two orders of magnitude more power at its disposal. The advantages of acoustic energy transfer compared to other sources of energy make it an appropriate choice for powering bio-implantable devices.

3. Acoustic power transfer

The devices shown in table 1, are specific instantiations and typically only tested at a single depth. This section will cover the physics of APT in order to provide a more complete picture of its potential. The basic structure of an APT system for a bio-medical implant is depicted in figure 5. An external ultrasonic transmitter converts electrical energy into a pressure wave which is transferred through the medium (i.e. body tissue). The pressure wave is captured by a receiver implanted in the body, and converted to electrical energy by an inverse process. A rectifier provides a usable stable DC voltage for powering a bio-sensor.

3.1. Fundamentals of acoustics

The field of physical acoustics deals with the generation and propagation of sound. A time-dependent external source can generate a perturbation into a gas, liquid, or solid in order to deliver momentum and energy to the medium. The propagation of the acoustic wave away from the source at a finite speed is a function of the elastic properties and density of the medium, and is governed by the wave equation [60].

The wave equation governing linear, lossless acoustic motion is derived for a linearized version of the principle of conservation of mass and momentum under the assumption of an isentropic equation of state [61]:

$$\frac{1}{c^2}\frac{\partial^2 p}{\partial t^2} - \nabla^2 p = 0, \qquad (1)$$

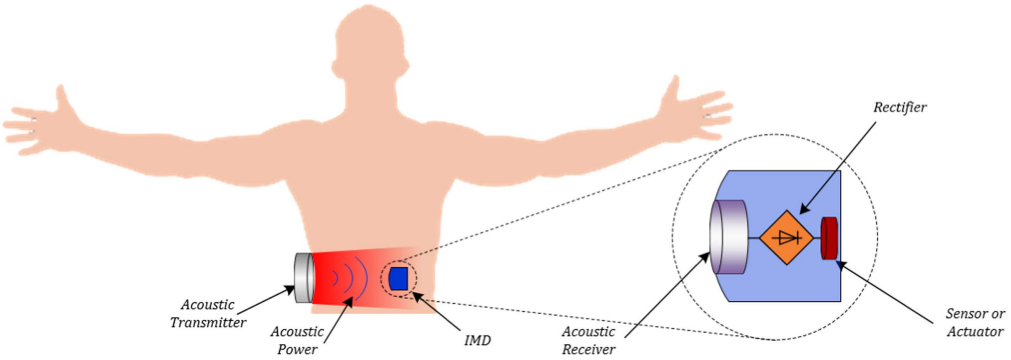

Figure 5. Diagram of an acoustic power transfer system for bio-medical implant.

Table 2. Mechanical properties of several materials used for acoustic transmission [63, 64].

Material	Density (kg m^{-3})	Acoustic velocity (m s^{-1})	Acoustic impedance (MRayls)
PZT	7500 ~ 8000	4000 ~ 5000	30 ~ 40
Water (20 °C)	1000	1480	1.48
Air (25 °C)	1.2	346	0.000 409
Human tissue	1490 ~ 1610	1060	1.58 ~ 1.7

where c is the isentropic speed of the sound and p is the acoustic pressure with respect to mean pressure. The pressure fluctuation, $p(x, t)$, can be derived as a function of the acoustic particle velocity, $u(x, t)$ for a plane, progressive acoustic wave propagating along the x-axis as [60]:

$$p(x, t) = \rho c u(x, t), \tag{2}$$

where ρ is the density of the medium and $Z = \rho c$ is the acoustic impedance of the medium. The SI unit of acoustic impedance is the Pa s m^{-1}, often called the rayl (1 rayl = 1 Pa s m^{-1} = kg s^{-1} m^{-2}). Acoustic impedance specifies how much pressure is generated by the vibration of the medium at the desired frequency. The acoustic impedance in a material is the product of its density and the speed of sound in the material [62]. The acoustic impedance for several materials can be found in table 2. It should be mentioned that some of the values for PZT and human tissue are reported as a range. This is due to the fact that there are several types of PZT materials as well as human tissue, and each of them has different properties. Moreover, the acoustic velocity depends on the direction in the material. As can be seen, there is a considerable mismatch between the acoustic impedance of piezoelectric material and tissue. In the case where there is a large impedance mismatch, a larger vibration amplitude would need to be generated by the transmitter in order to push the desired acoustic power to the tissue than with a matched transducer. This issue will be fully covered in the impedance matching section.

The instantaneous acoustic intensity, $\vec{I}(x, y, z, t)$, is defined as the power per unit area and can be calculated by knowing the acoustic particle velocity vector $\vec{u}(x, y, z, t)$ [60]:

$$\vec{I}(x, y, z, t) = p(x, y, z, t)\vec{u}(x, y, z, t). \tag{3}$$

The corresponding acoustic power W of the source can then be found by integrating the intensity over the source area.

The characteristics of the generated pressure field in a medium change with distance from the transmitter. The pressure field is generally split into the near field and far field. In the near field, for a cylindrical transmitter, the shape of the pressure field is cylindrical and the pressure magnitude oscillates with distance from the transmitter having multiple minima and maxima which make the power transfer unpredictable [35]. In other words, the perturbation to the transmitter, which is caused by having an object in its near field, makes it hard to predict the transferred power. At a certain distance from the transmitter on the acoustic axis, the beam begins to diverge and the pressure field changes to a spherically spreading wave which decays with increasing distance. The far field is generally smoother than the near field with pressure decaying with distance. At the transition between the near field and far field, as seen in figure 6, the pressure field converges to a natural focus. This transition distance is called the Rayleigh distance and is defined as [65]:

$$L = \frac{(D^2 - \lambda^2)}{4\lambda} \approx \frac{D^2}{4\lambda}, D^2 \gg \lambda^2, \tag{4}$$

where D is the aperture width of the source or transmitter and λ is the wavelength of the acoustic wave in the medium, which is a function of frequency, f.

The wavelength, λ, is defined as:

$$\lambda = \frac{c}{f}. \tag{5}$$

At the Rayleigh distance, for circular transducers, the acoustic beam spreads out at an angle that can be calculated

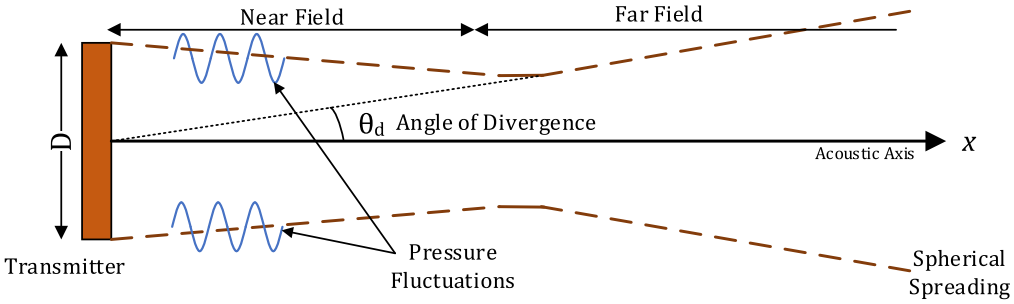

Figure 6. Representation of near field and far field.

by the wavelength and the diameter of the transmitter as:

$$\theta_d = \sin^{-1}\left(\frac{1.22\lambda}{D}\right). \tag{6}$$

By knowing the intensity at zero distance, $I(0)$, the intensity distribution for each point on the propagation axis can be given by:

$$I(x) = I(0)\sin^2\left[\left(\frac{\pi}{\lambda}\right)\left(\sqrt{\frac{D^2}{4} + x^2} - x\right)\right]. \tag{7}$$

In order to achieve the maximum received power, it is best to place the receiver at one Rayleigh distance where the beam spreading is at a minimum [66], and the acoustic pressure has a large and stable value. On the acoustic axis in the near field, there are several points at which the pressure has its maximum value. The location of these points depends on the wavelength and the diameter of the transmitter. Considering m as the order of the pressure peak, the pressure peak locations can be calculated as [35]:

$$X_{\max}(m) = \frac{D^2 - \lambda(2m+1)^2}{4\lambda(2m+1)} \quad m = 1, 2, 3, \ldots. \tag{8}$$

3.2. Impedence matching

When there is an impedance mismatch for a wave generated by a transducer with acoustic impedance Z_2 propagating in a medium with acoustic impedance of Z_1, a reflection coefficient, for normal incidence, can be defined as [64]:

$$\Gamma = \frac{Z_2 - Z_1}{Z_2 + Z_1} = \frac{P_r}{P_i}. \tag{9}$$

The reflection coefficient can be interpreted as the ratio of the amplitude of the reflected wave P_r to the amplitude of the incident wave $_{Pi}$. Therefore, the transferred pressure wave will be $P_t = (1 - \Gamma)_{Pi}$. This means that the larger the reflection coefficient value, the smaller the captured wave by the receiver. According to table 2, there is a mismatch between the acoustic impedance of PZT (39.71 MRayls) and average value for human tissue (1.64 MRayls), and therefore, the reflection pressure coefficient will be 0.92. Therefore, only $(1 - \Gamma) = 0.08$ of the generated wave is captured by the receiver. The situation is actually worse as the power depends on P_t squared which is proportional to $(1 - \Gamma)^2$. In other words, the intensity of the reflected wave I_r depends on the square of Γ and can be written as:

$$\frac{I_r}{I_i} = |\Gamma|^2. \tag{10}$$

Another concern with mismatched impedances is the generation of pressure standing waves in the tissue by the reflected wave [61]. As discussed in the previous section, this problem can cause peak pressure levels that exceed the tissue safety limit. Hence, in order not to exceed the tissue safety limit and to avoid any losses in the transferred power, it is necessary to match the transducer impedance to the tissue impedance.

Acoustic impedance matching techniques can generally be classified as either single or multiple matching layer methods. The single matching layer method is the easiest and the most common technique. Using this method, a layer with a thickness of $\lambda/4$ is inserted between the transducer and the medium. It should be mentioned that this single matching layer technique using a layer with a thickness of $\lambda/4$ works well at a single frequency and is not broadband. The inserted layer should be biocompatible and have an acoustic impedance close to [35]:

$$Z_{\text{matching}} = \sqrt{Z_1 \,.\, Z_2}. \tag{11}$$

The main disadvantage of using the single layer matching technique is that it considerably limits the availability of a biocompatible material with the calculated acoustic impedance. For the case of PZT and tissue, the calculated acoustic impedance is 8.1 MRays, and there are few biocompatible materials with this acoustic impedance value. Another issue of this method is that it does not consider the adhesion layer between the transducer and the new material which can negatively affect the quality of matching. Of course, its effect on the matching layer is negligible if the adhesion layer thickness is thin compared to the matching layer thickness.

Alternatively, multiple layers for matching the acoustic impedances of the transducer and tissue can be used [63, 67–69]. Each of the matching layers and their adhesive layers are represented by a 2×2 matrix. The acoustic impedance

matching is then obtained by the multiplication of a chain of transfer matrices. For the nth layer with acoustic impedance of Z_n, the transfer matrix is defined by [69]:

$$T_n = \begin{bmatrix} \cos\theta_n & jZ_n \sin\theta_n \\ \frac{j}{Z_n}\sin\theta_n & \cos\theta_n \end{bmatrix}, \tag{12}$$

where $\theta_n = 2\pi t_n/\lambda_n$ is the phase shift, and t_n is the thickness of nth layer. Then, the equivalent matrix T_{equ} can be obtained by multiplying the transfer matrices for each layer as:

$$T_{\text{equ}} = T_1 T_2 \ldots T_n = \begin{bmatrix} T_{11} & T_{12} \\ T_{21} & T_{22} \end{bmatrix}. \tag{13}$$

When the equivalent acoustic impedance of all the layers equals the acoustic impedance of the tissue, matching is obtained. Assuming Z_1 to be the acoustic impedance of the transducer, the equivalent acoustic impedance resulting from multi layers is then given by:

$$Z_{\text{equ}} = \frac{T_{11}Z_1 + T_{12}}{T_{21}Z_1 + T_{22}}. \tag{14}$$

Finally, it should be noted that the effective acoustic impedance of the receiver can be adjusted through the electrical impedance of the load circuitry [28]. The acoustic impedance of bulk ceramics is more or less constant. However, the acoustic impedance of poled electroceramics depends strongly on the frequency near resonance. Thus, the acoustic impedance is a function of both the frequency and electrical load [35, 70].

3.3. Frequency selection

It is important to select a proper transmission operating frequency as several critical operational factors can be negatively impacted by improper selection, such as tissue attenuation, Rayleigh distance, and the size of the receiver and transmitter. The best choice is to use the resonance frequency of the transducer and operate the transducer close to this frequency in order to achieve the maximum transferred power. The resonance frequency of the transducer depends on the geometry and material of the transducer. By increasing the frequency, the thickness of transducers and matching layer decrease. However, the Rayleigh distance increases with frequency, which leads to an increase of losses due to tissue absorption.

Both the frequency and the intensity of the acoustic field affect safety. The FDA states that for continuous energy transfer through tissue, the spatial-peak temporal-average intensity (I_{SPTA}) should be less than 7200 μW mm^{-2} to avoid any thermal damage [48]. In order to address mechanical damage, the FDA limits the spatial-peak peak-average intensity (I_{SPPA}) for pulse wave telemetry and energy delivery to be less than 190 W cm^{-2} [48]. Finally, in order to measure and estimate ultrasonic bio-effects, the mechanical index (MI) is defined as [71]:

$$\text{MI} = \frac{p_n}{\sqrt{f_c}}, \tag{15}$$

where p_n is peak negative pressure of the ultrasound wave in MPa, de-rated by 0.3 dB cm^{-1} MHz^{-1} to account for the difference between in-water and in-tissue acoustic attenuation, and f_c is the center frequency of the ultrasound wave in MHz. MI is an indication of an ultrasound beam's ability to cause cavitation related bio-effects, and can be considered as a reasonable proxy for micro mechanical damage. A higher MI produces a larger bio-effect (cavitation) [59]. Therefore, cavitation is less prominent at high frequencies whereas lower frequencies can be less safe. To reduce the risk of cavitation for diagnostic ultrasound, the FDA states that the MI must be lower than 1.9 [48].

Other parameters that can be affected by the operating frequency are the attenuation factor α and the loss of pressure amplitude. The pressure can be expressed as [59]:

$$p(x) = p_0 \exp^{-\alpha(f)x}, \tag{16}$$

where the attenuation factor $\alpha(f) = \alpha \times f_0^{\,k}$ is a function of operating frequency. The average attenuation coefficient for biological soft tissue α is considered to be 0.3 dB cm^{-1} MHz^{-1} [72, 73]. The distance along the acoustic axis is x, and k is a constant with a value of 1 for tissue. The normalized pressure ($p(x)/p_0$) exponentially decreases with increasing operating frequency for a constant distance. Hence, higher frequencies limit the penetration of ultrasound and promote heating.

3.4. Transducer structures

Although there is a wide variety of possible transduction methods to convert acoustical to electrical energy, only a few are frequently used in practice. Most acoustic power generators employ electrostatic [74, 75] or piezoelectric [28] transduction methods. Piezoelectric transduction is the most common method used for receiving acoustical energy and converting it to electrical energy [60] and vice-versa. Figure 7 shows two common types of piezoelectric architectures which can be used for APT: the bulk-mode plate and the flexure-mode unimorph diaphragm. The plate is a circular piezoelectric disk that is usually fixed around its circumference. The piezoelectric 3–3 axis, which is the poling axis, is perpendicular to the face of the plate. The diaphragm is also a circular piezoelectric disk. However, one face of the piezoelectric disk is fixed to the back side of a larger circular elastic layer, or shim that is not piezoelectric. The shim is clamped around its circumference. Figure 7 shows two different diaphragm architectures. Diaphragm structures can be made with a single piezoelectric layer (i.e. a unimorph), or a piezoelectric layer on each side of the shim (i.e. a bimorph). The piezoelectric layer can either partially cover the shim or cover the entire surface of the shim and employ patterned electrodes on the piezo surface. If implemented as a MEMS device, this structure is usually referred to as a piezoelectric micromachined ultrasound transducer or PMUT.

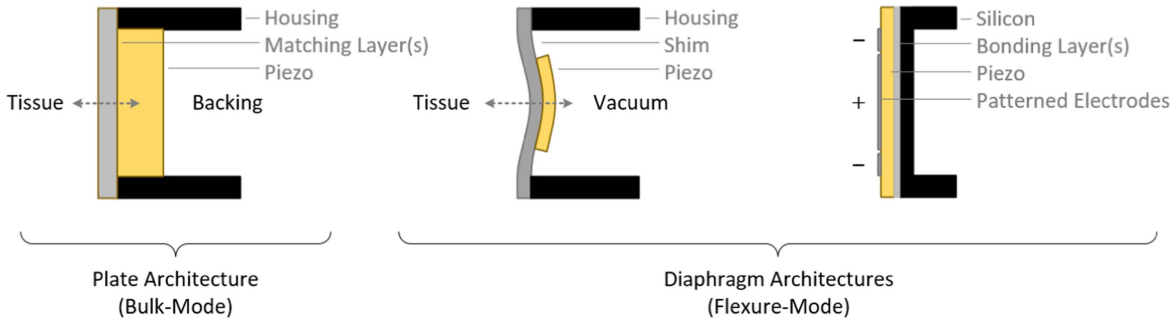

Figure 7. Plate (left), unimorph diaphragm (middle), and patterned-electrode PMUT diaphragm (right) architectures.

The literature is focused more on the plate architecture for transferring power in an implantable device. There are two main reasons that the plate structure can have better performance compared to the diaphragm. First, the diaphragm structure operates in 3–1 mode which, for most materials, has a lower coupling coefficient compared to the 3–3 mode of the plate. Second, plates use significantly more piezoelectric material than diaphragms of the same diameter and thus have better performance in terms of acoustic to electric generation. However, diaphragm structures can operate at much lower frequencies for a given diameter leading to less signal attenuation and tissue heating which can make them appealing for bio-implantable power applications. Christensen and Roundy [28] analyzed these two structures as implantable acoustic receivers for powering small, deeply implanted devices, and compared the power loss mechanisms and the total power generated for these two structures. They showed that the diaphragm architecture generates more power compared to plate architecture for large implant distances and small device sizes. They also concluded that the diaphragm is generally less sensitive to misalignment and differences in orientation.

Piezoelectric materials are widely applied in a variety of macroscale devices; however, their integration into microsystems has been challenging. Among lead zirconate titanate (PZT), zinc oxide, and aluminum nitride, PZT is the dominant piezoelectric material for power generation purposes in the literature [3] given that it exhibits higher piezoelectric coefficients, d_{33}, d_{31}, and coupling coefficients [76]. Existing deposition techniques for integration of piezoelectric materials on silicon are introduced in [77] and their challenges are discussed. As bulk piezoelectric materials provide much more electromechanical force due to the simple fact that they contain more piezoelectric material, maximum power generation is usually obtained with bulk materials rather than thin-film deposited piezoelectric materials.

4. Modeling techniques

Design optimization and analysis of acoustic energy harvesting devices require some form of modeling (analytical or numerical) to predict behavior. The basic equations of acoustics, which can be used to develop analytical models, are discussed in the fundamentals of acoustics section. Either analytical or numerical modeling, or a combination of both, may be appropriate for a given power transfer design depending on the structures, transduction techniques, and accuracy required. The lumped element modeling technique attempts to capture spatially distributed phenomena by discretizing elements into lumped components. This technique is conducive to creating equivalent electrical circuits. It is easy implement and thus can be used as the first modeling technique to predict the behavior of the system and to analyze the impact of each parameter on the system response. Numerical methods are also used, particularly when the complexity or required accuracy exceeds the capabilities of lumped element or simplified analytical models. It is important to note that lumped element models are one dimensional, and therefore other modeling techniques, such as numerical methods, should be considered for modeling the whole system in three dimensions to further investigate behavior.

4.1. Lumped element modeling (LEM)

A popular method to model acoustic signal or power transfer is by electrical circuit analogy. By developing equivalent lumped parameter components, this modeling method allows one dimensional analysis. It also enables simulation using a large infrastructure of circuit simulation tools [78]. As most acoustic energy harvesting systems use piezoelectric transducers, the classical Krimholtz, Leedom, and Matthae (KLM) [79] and Mason [80] equivalent circuit models are two attractive and common methods for modeling the piezoelectric plate architecture. Mason first developed an electrical equivalent circuit model by treating acoustic wave propagation as an electrical transmission line as illustrated in figure 8. KLM developed a similar equivalent circuit model, shown in figure 9, in part to replace the negative capacitance, which is not a physical device, in the Mason model. However, it has been shown that these two models produce equivalent results [81] and can be used interchangeably. These models can be treated as a starting point to develop a full model with all the system constraints. The entire piezoelectric transducer with two electrodes on its largest faces is modeled as a frequency dependent three-port network. The models include one electrical port for applying or collecting electrical power, and two acoustical (or mechanical) ports for generating or receiving mechanical waves as shown in figures 8 and 9. In the

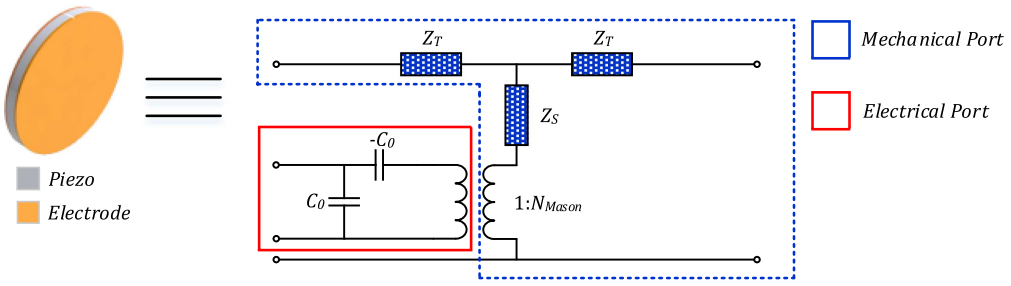

Figure 8. Mason equivalent model of a piezoelectric transducer.

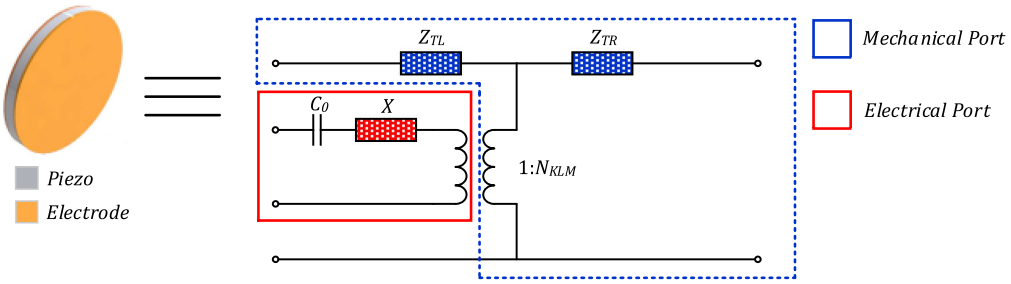

Figure 9. KLM equivalent model of a piezoelectric transducer.

mechanical port, the acoustic impedances due to the two faces of the piezoelectric transducer are modeled as quarter wavelength transmission lines [82]. The effect of matching layers can also be modeled as an acoustic impedance in series with the acoustic impedances of the transmitter and the receiver. The piezoelectric transducers for these models are generally plates operating in thickness stretch mode, however, there are formulations for other very simple geometries [83].

The frequency dependent acoustic capacitance, X, will become zero when the system operates at the series resonance frequency f_r which is [82]:

$$f_r = \frac{c}{2d}, \tag{17}$$

where c is the acoustic velocity in the piezoelectric transducer, and d is its thickness. For a specific area of the piezoelectric material (A), it can be shown that the acoustic impedance is:

$$Z_0 = \rho A c = A\sqrt{\rho c_{33}^D}, \tag{18}$$

where $c^D{}_{33}$ is the open circuit complex elastic stiffness. According to figure 9, C_0 represents the transducer capacitance. In other words, C_0 is the parallel-plate capacitance from the electrodes and is given by:

$$C_0 = \frac{\varepsilon_{33}^S \cdot \varepsilon_0 A}{d}, \tag{19}$$

where ε_0 is permittivity of free space, and $\varepsilon^S{}_{33}$ is the clamped relative complex permittivity. An ideal transformer with a turn ratio of N is considered for modeling the transduction between electrical and mechanical domains. The turn ratio for the Mason and KLM models can be expressed as follows [82]:

$$N_{\text{Mason}} = \frac{C_0}{h_{33}}, \tag{20}$$

$$N_{\text{KLM}} = \frac{1}{2\left(\frac{h_{33}}{\omega Z_0}\right)}\csc\left(\frac{kt}{2}\right), \tag{21}$$

where h_{33} is the piezoelectric pressure constant, defined by [82]:

$$h_{33} = k_t\sqrt{\frac{c_{33}^D}{\varepsilon_{33}^S \cdot \varepsilon_0}}, \tag{22}$$

where k_t is the electromechanical coupling coefficient. The other circuit parameters, shown in figure 8, for the Mason model are defined as [81]:

$$Z_T = iZ_0 \tan\left(\frac{kt}{2}\right), \tag{23}$$

$$Z_S = -iZ_0 \csc(kt). \tag{24}$$

The values for the impedance elements of KLM model, shown in figure 9, can be given by [81]:

$$Z_{TL} = Z_0\left[\frac{Z_L \cos\left(\frac{kt}{2}\right) + iZ_0 \sin\left(\frac{kt}{2}\right)}{Z_0 \cos\left(\frac{kt}{2}\right) + iZ_L \sin\left(\frac{kt}{2}\right)}\right], \tag{25}$$

$$Z_{TR} = Z_0\left[\frac{Z_R \cos\left(\frac{kt}{2}\right) + iZ_0 \sin\left(\frac{kt}{2}\right)}{Z_0 \cos\left(\frac{kt}{2}\right) + iZ_R \sin\left(\frac{kt}{2}\right)}\right], \tag{26}$$

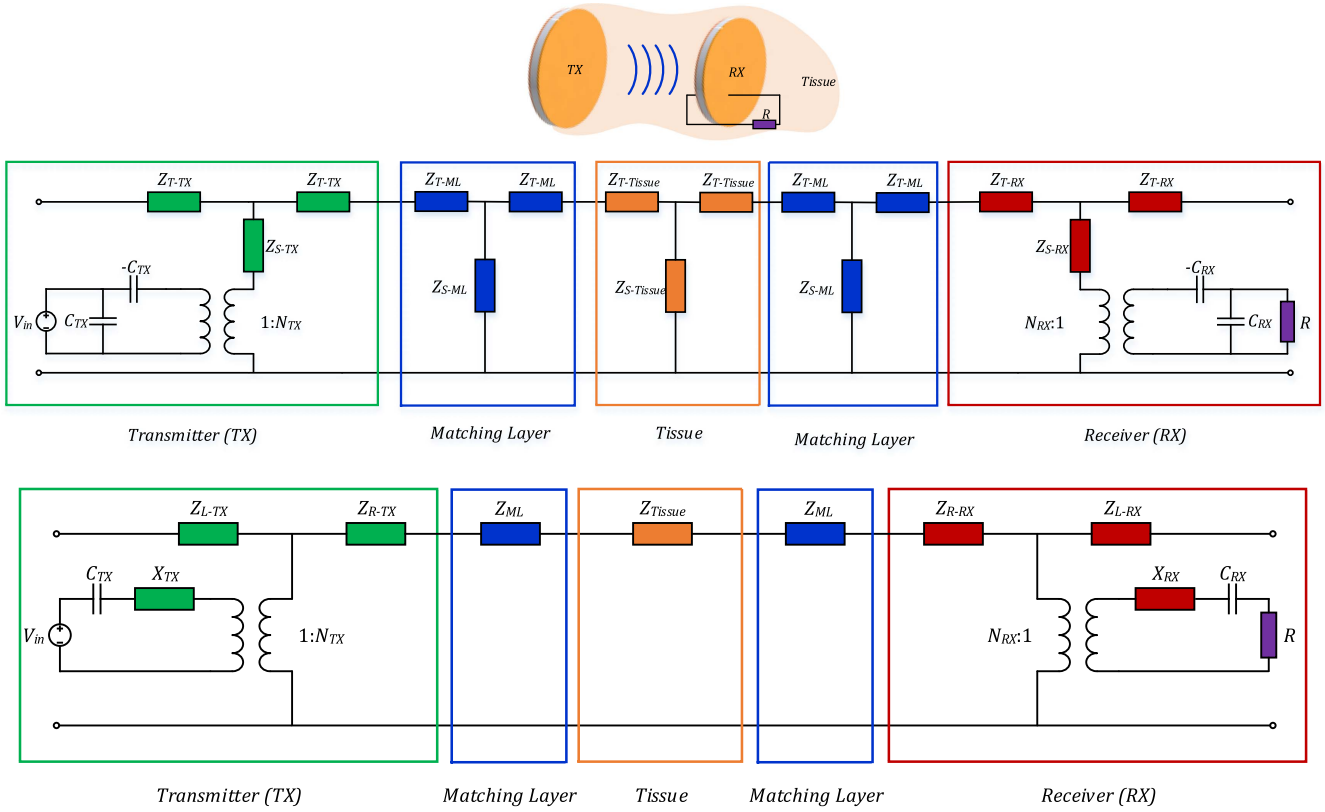

Figure 10. Complete LEM model for an acoustic power transfer system using the Mason (top) and KLM (bottom) models.

$$X = \mathrm{i}Z_0\left(\frac{h_{33}}{\omega Z_0}\right)^2 \sin\left(\frac{kt}{2}\right), \tag{27}$$

where Z_{L} and Z_{R} are the load impedance on left and right acoustic ports, respectively. The output power of the system, which is delivered to the load R, can be calculated by using the Thevenin equivalent model and assuming operation at the resonance frequency. In the Thevenin equivalent model, there is an output impedance $Z_{\mathrm{out}} = 1/j\omega C_{\mathrm{RX}}$,where C_{RX} is the capacitance (i.e. C_0) of the receiver. The load R is the electrical load impedance at the receiver. Therefore, the power can be derived as follows [82]:

$$P_{\mathrm{out}} = \frac{1}{2C_{\mathrm{RX}}}\left(\mu T \,.\, N \,.\, \frac{R}{R + Z_{\mathrm{out}}}\right)^2 .\, f_{\mathrm{r}}, \tag{28}$$

where $T \approx 2\left|Z_{\mathrm{Receiver}}\right| \times c$ and μ is the tissue attenuation ($\mu = \mathrm{e}^{-2\alpha x}$, α is the attenuation coefficient and x is the depth of the implant). Z_{Receiver} is the acoustic impedance of the receiver in the mechanical port. Finally, knowing the C_0 of the transmitter, or C_{TX}, the theoretical power efficiency (η) is defined as [82]:

$$\eta = \left|\frac{P_{\mathrm{out}}}{P_{\mathrm{in}}}\right| = \frac{\left(\mu T \,.\, N \,.\, \dfrac{R}{R + Z_{\mathrm{out}}}\right)^2}{C_{\mathrm{TX}} C_{\mathrm{RX}} V_{\mathrm{in}}^2}, \tag{29}$$

where P_{out} and P_{in} are the electrical output power delivered to the load and the electrical input power to the transmitting transducer, respectively. The complete equivalent circuits of an APT system using the Mason and KLM models are illustrated in figure 10.

4.2. Numerical approaches

Huygens principle is one approach to calculating the pressure generated by an ultrasound transducer at some location away from the transducer. Using this principle, each vibrating point on the surface of the transmitter is considered as the center of a new disturbance which acts as a point source emitting a spherical wave. It is assumed that propagation from these sources is forward. For a circular piston transmitter with radius a, the total acoustic pressure at an observation point on the acoustic axis with distance x from transmitter due to radiation from all incremental areas ds is [84]:

$$p = -j\rho_0 u f \int_0^{2\pi}\int_0^{a} \frac{\mathrm{e}^{j\frac{\omega}{c_0}(l - c_0 t)}}{l} r \mathrm{d}r\mathrm{d}\varphi, \tag{30}$$

where r is the distance from the origin to ds, u is the particle velocity at ds, and l is the distance from each incremental area to the observation point, shown in figure 11 and calculated by:

$$l = \sqrt{r^2 + x^2}\,. \tag{31}$$

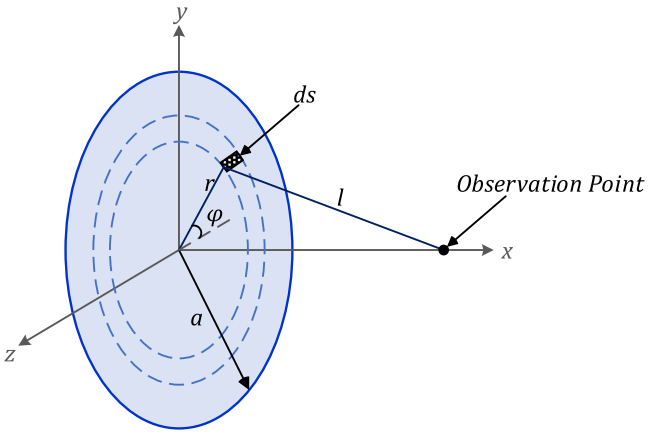

Figure 11. Geometry of a circular transmitter.

By integrating over the surface of the transmitter, the pressure at the observation point can be derived as:

$$p = (-2j\rho_0 c_0 u)\left[\cos\left(\frac{\omega}{2c_0}(\sqrt{a^2+x^2}+x)\right) + j\sin\left(\frac{\omega}{2c_0}(\sqrt{a^2+x^2}+x)\right)\right]e^{-j\omega t} \times \sin\left(\frac{\omega}{2c_0}(\sqrt{a^2+x^2}-x)\right). \quad (32)$$

Finite element method (FEM) simulations are implemented in order to validate design concepts and to provide useful physical insights. Moreover, when using these techniques, one can straightforwardly carry out design optimization to improve the output voltage or to reduce device size. There are several works in the literature which make use of commercial FEM software such as COMSOL. As these problems deal with several areas of physics, including acoustics, solid mechanics, and piezoelectricity, COMSOL seems to be a good candidate since it has many features useful in solving multi-physics problems.

Ozeri *et al* used COMSOL to carry out a 2D axisymmetric simulation [35, 36]. Their simulation model included the piezoelectric element with its acoustic matching layer. Simulations were done for a maximum propagating distance of 50 mm surrounded by a thin perfectly matched layer to avoid reflections. Other works include the use of COMSOL to extract the effective acoustic impedance of the receiver in order to include the effect of resonance shift in the KLM model [66].

Shahab *et al* [85, 86] used finite element simulations to compare to an analytical model for ultrasonic power transfer. Their presented analytical model is a continuum model that is capable of modeling a cylindrical receiver excited by a spherical wave source. The simulation was carried out in COMSOL to explore the 3D behavior of the receiver in water under harmonic excitation. The longitudinal tip displacement and the output voltage of the receiver were both computed using the analytical and FEM model and were compared to each other. They report that good agreement was observed in these results.

ANSYS, another computer aided engineering software tool, is also used by some researchers to model their devices. Hori *et al* developed a two-dimensional axisymmetric model in ANSYS in order to investigate optimal design parameters. Their model includes the piezoelectric element and the matching layer, and the propagating medium is assumed to be water and modeled as an infinite medium [87]. Other published works use ANSYS for modeling only a part of the power transfer system. For instance, He *et al* [88] simulated their MEMS device in ANSYS to find the resonance frequency of the receiver.

k-Wave is an open source Matlab toolbox designed for the time-domain simulation of propagating acoustic waves in 1D, 2D, or 3D [89]. The toolbox can model both linear and nonlinear wave propagation based on numerical models. It is also capable of performing photoacoustic reconstruction and modeling elastic wave propagation in solids.

The modeling techniques discussed thus far are primarily geared toward piezoelectric transducers. However, other transduction mechanisms, most notably electrostatics, have been used for APT in the context of IMDs. Capacitive micromachined ultrasound transducers (CMUTs) have been employed to receive the mechanical wave and convert it to electrical energy. For instance, Fowler *et al* developed a CMUT device and implemented the modeling in CoventorWave, which is a MEMS design software package for finite element analysis [90].

Table 3 presents a summary of different modeling techniques used by researchers for modeling APT for implants. Basic equations and analytical methods, in general, are not attractive to model complex systems. LEM techniques are still popular as they are easy to implement and can model the whole APT system as a circuit. Among numerical methods, COMSOL appears to be to the most widely used among researchers. Finally, the finite difference time domain (FDTD) method also provides full-wave solutions to the propagation problem [91]. Mo *et al* used this technique to study the effect of misalignment of the ultrasound transmitter and receiver on the power transmission efficiency [92].

5. Reported devices

Several research groups are currently active in the field of APT for bio-medical devices, and a wide range of devices have been reported. Here we summarize some of the key developments and trends, with examples for each of the main device types.

5.1. Electrostatic transduction

Significantly less work has been reported on electrostatic transduction than on piezoelectric transduction, possibly because of the lower achievable output power. These devices most often employ a comb drive to generate electrical energy from a base vibration. Depending on the actuation

Table 3. Different modeling techniques used by published works.

Article		Analytical		LEM		Numerical				
Author	Year/Ref	Basic equations	Continuum	Mason	KLM	Huygens	COMSOL	ANSYS	CoventorWare	FDTD
Arra	2007/[56]	●								
Ozeri	2010/[35]	●			●		●			
Denisov	2010/[29]			●						
Zhu	2010/[74]								●	
Shigeta	2011/[93]			●				●		
Ozeri	2012/[94]						●			
Seo	2013/[65]				●					
Mo	2013/[92]									●
Hori	2013/[87]			●				●		
Fowler	2013/[95]								●	
Lee	2013/[96]					●				
Lee	2014/[97]					●				
Fowler	2014/[90]								●	
He	2014/[88]							●		
Shahab	2014/[98]		●				●			
Ozeri	2014/[70]	●			●					
Chou	2014/[99]				●		●			
Fowler	2015/[100]								●	
Charthad	2015/[45]				●		●			
Christensen	2015/[28]	●		●						
Song	2015/[82]				●					

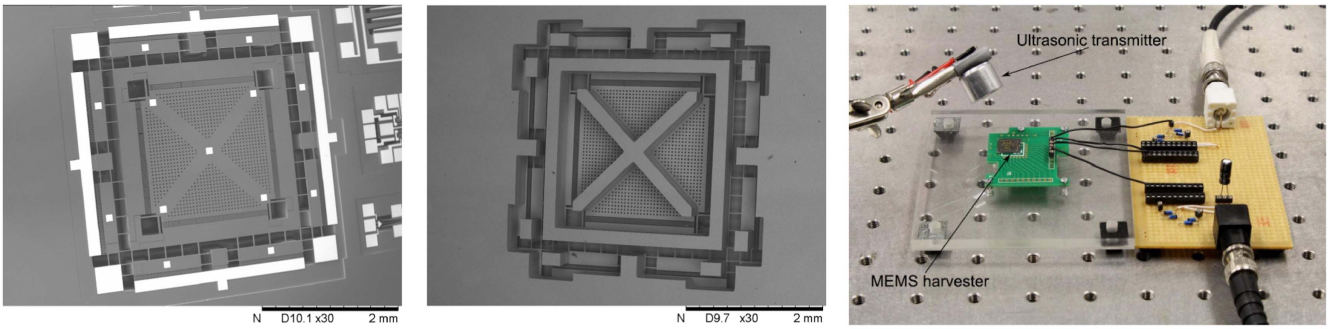

Figure 12. (a) SEM image of fabricated MEMS energy harvester, (b) underside of fabricated harvester, (c) photo showing MEMS harvester experimental setup [90].

mechanism, there are three types of electrostatic harvesters including in-plane gap closing, in-plane overlap, and out-of-plane gap closing electrostatic generators [3]. For the in-plane gap closing generators, the actuation direction can be parallel or perpendicular to the plane. The highest power density can be achieved from in-plane gap closing electrostatic generators since their design is more manageable and less prone to detrimental in-plane rotation [101].

Moheimani *et al* one of the only groups publishing on electrostatic transduction for IMDs, have reported a MEMS device that vibrates due to incoming ultrasonic waves for extracting ultrasonic energy via electrostatic comb-finger transducers. For a proof of concept in 2010, they developed a two degree-of-freedom (2-DOF) device capable of generating power of up to 21.4 nW for an air gap of 5 mm [74, 102]. The fabrication process was based on a commercial silicon-on-insulator (SOI) MEMS process with a 25 μm thick device layer and minimum gap of 2 μm which is fully presented in [103]. In 2013, they designed and fabricated a 3-DOF CMUT device, shown in figure 12, that has three resonance modes in three different translational directions so that ultrasonic energy can be harvested regardless of the device's orientation relative to the exciting ultrasonic transmitter [90, 95]. The resonance frequency of their fabricated device was around 25 kHz, and the device can generate 24.7, 19.8, and 14.5 nW in each of three directions from ultrasonic waves generated by an external transmitter. Adding a rotational mode to their device improved the total output power in two directions [100]. This device provided average power outputs of 50.9, 60.6, and 14.3 nW in three directions. Although these power values are still low, they may be useful for certain implanted medical devices including pacemakers, neurostimulators, and drug pumps.

5.2. Piezoelectric transduction

5.2.1. Plate structure. A plate structure for transmitting and receiving power is most commonly used in the literature. In 2001, Kawanabe *et al* developed a device with two piezo discs [104]. The rectified output power of their devices can be used to charge the battery of a cardiac pacemaker. They also studied the temperature increase in the body due to the input power since their input power is relatively high (0.5 and 1.7 W). For an input power of 1.7 W, the temperature inside the skin started to increase from about 35 °C–36.5 °C in 25 min. A power of 340 mW could be transferred with their device with an efficiency of 20%. The same research group presented a modified structure with two pairs of piezo oscillators [105]. This newer device increased the information transmission rate from 600 bps to 9.5 Kbps. Although it applied six times higher input power compared to their previous work, they have not studied the resulting temperature change inside the body. The efficiency of the device was the same as their previously reported device which results in higher output power and voltage.

In order to power implantable devices with a power level up to a few hundred mW, Ozeri *et al* developed an ultrasonic receiver operating at 673 kHz [35]. The transducers contain matching layers consisting of two layers of cyanoacrylate and graphite. Their models include the effect of the matching layers. They investigated the output power for different receiver depths ranging from 5–30 mm through water and pig muscle in a test tank. They also studied the effect of lateral misalignment of the transducers. According to their results, the efficiency of the power transfer through pig muscle is much smaller than the efficiency through water since pig muscle has more than two orders of magnitude higher attenuation compared to water. To improve the efficiency of their system, Ozeri *et al* presented a transducer based on a kerfless transmitter with Gaussian radial distribution of its radiating surface velocity [36]. The efficiency increased from 27% to 39.1% by partitioning the transmitter electrode in to five concentric rings in order to have six equal area concentric elements.

Lee *et al* [96] describe an ultrasound power transfer system in which the frequency is adjusted in order to maximize the power transfer efficiency for different tissue thicknesses. For instance, at a 23 mm depth, the maximum efficiency was achieved at 255 kHz which is 21% while the maximum power transfer efficiency at a 45 mm depth was 13.8% at 265 kHz.

Ziaie *et al* developed an implantable micro-oxygen generator with the total size of 1.2 mm × 1.3 mm × 8 mm [46]. Instead of PZT disks, they used a PZT bar whose dimensions are chosen in a way to compromise between the

size of the implant and body attenuation. The whole device was covered by a 5 μm-thick parylene layer for biocompatibility assurance. An implantable pressure sensing system was also presented by this group [106]. Their fabricated prototype, which was used for measuring bladder pressure, has a diameter of 8 mm and a length of 40 mm. A speaker with input power of 11.7 W was used to generate an acoustic wave resulting in an output power of 16 μW. It should be noted that APT under angular misalignments of the receiver was also studied.

Mazzilli *et al* have also worked on ultrasound wireless energy transfer for implantable medical devices. They used focused transducers in order to narrow the ultrasonic beam in the near field and increase the output power intensity. In 2010, they presented a power transfer system with a single element focused transducer having a diameter of 50 mm and a radius of curvature of 50 mm as the transmitter, and a receiver with a diameter of 6.35 mm [107]. Operating at a frequency of 1.033 MHz, they achieved a power transfer of 3 mW with an electro-acoustic efficiency of 10%. In another work, they used a plate array for the receiver and a spherical array for the transmitter [59]. A spherical transducer array made up of 64-elements was employed for the transmitter to focus the transmitting beam. The receiver was an array of six elements, each with an area of 1 mm $\times$ 5 mm. The output power of this device was 28 mW with the efficiency of 1.6%.

5.2.2. Diaphragm structure. The plate structure is an efficient structure as long as the piezoelectric device can be relatively thick. For optimal performance, the piezoelectric thickness should be half the acoustic wavelength in the piezoelectric material. The acoustic wavelength in PZT at 1 MHz is approximately 4 mm. In order for the piezoelectric element to be much thinner (significantly below 1 mm) and operate efficiently, the frequency must go up. However, as the frequency goes up, so does the absorption in tissue [108]. For this reason, some researchers are studying the use of piezoelectric devices with alternative, more compliant, geometries as power receivers. This will enable a thinner device to be used efficiently at lower frequencies resulting in increased overall efficiency. It should be noted that compliant diaphragm structures are used as ultrasound transceivers, external to the body, for imaging applications [109]. However, the imaging application is significantly different than an implanted power receiver.

Lee *et al* developed a diaphragm based PZT receiver and conducted acoustic transmission experiments with it using streaky pork at four different depths [110]. They achieved a maximum power output of 0.15 μW at a resonance frequency around 1.5 kHz. As part of this work, they developed a novel customized PZT deposition chamber based on a jet-printing method for implantable power harvesters. The thickness of the deposited PZT is about 10 μm, which is achieved by depositing PZT powders with particle size smaller than 1 μm in diameter which were put in a continuously vibrating powder container. The same group also studied the effect of packaging on the output voltage [111, 112]. Two different spherical and cubic packages with the same cross section were considered. The packaged and unpackaged devices were tested in different mediums such as air, fatty, and muscular pork tissue. The maximum power transmission efficiency was achieved when using the spherical package in the muscular layer of the streaky pork.

As stated earlier, the integration of piezoelectric materials to microsystems suffers from several weaknesses of additive thin-film deposition methods. Current deposition methods for piezoelectric materials on a silicon wafer such as sol–gel [113], sputtering [114], screen printing [115], and pulsed laser deposition [116] result in lower piezoelectric material performance compared to bulk PZT. Furthermore, the PZT films are thin (typically $<$5 μm). Thicker films would result in higher power generation capability. Some other issues include high-temperature deposition steps and issues related to film uniformity and process reliability [77]. Therefore, alternative fabrication methods have been introduced to fabricate thick film piezoelectric receivers for energy harvesting and power transfer applications.

Aktakka *et al* [77, 117, 118] developed a low-temperature, aligned, wafer scale bonding process to integrate commercially available piezoelectric substrates on silicon, which appears to be an appropriate process for fabricating implanted piezoelectric receivers. They have presented a low-temperature (200 °C) gold–indium bonding process for bulk PZT wafers on Si wafers. PZT films with a thickness of 10 μm were achieved using mechanical lapping and polishing. They report the fabrication of both square and circular shaped PZT diaphragms with three different sizes.

He *et al* [88] used a MEMS fabrication processes to fabricate the ultrasonic PZT receiver for implantable micro-devices shown in figure 13. The fabrication process, [119], makes use of a low-temperature bonding technique using conductive epoxy resin, after which the bulk PZT is thinned using mechanical lapping. As they developed a device with a PZT layer with a thickness of 40 μm through bonding and mechanical thinning methods. The operating frequency is about 40 kHz which is considerably lower than reported plate structures.

Christensen and Roundy [28] have recently carried out a comparative study between plate and diaphragm piezoelectric receivers for implantable devices. The results of their modeling, which were validated on larger devices, indicate that more power can generally be achieved by a diaphragm structure compared to a plate structure for diameters of approximately two millimeters and smaller. They also concluded that the diaphragm is significantly less sensitive to changes in implant depth, alignment, and orientation.

5.3. Power transfer performance metrics

We consider three different performance metrics, or figures of merit, in comparing different devices. Efficiency can be defined as the ratio of generated output electrical power from the receiver to electrical input power applied to the transmitter and is expressed as a percentage. Although it can give good insight into the effectiveness of power transfer, it does not

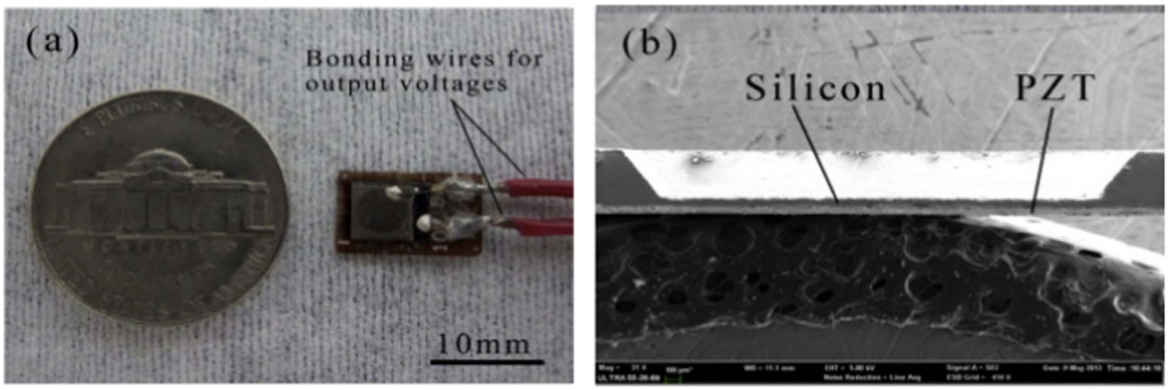

Figure 13. (a) Optical image of receiver and (b) SEM image of the cross-section of the receiver [88].

consider the dependence of input and output power to the device size. In other words, the best efficiency is usually achieved when the transmitter and receiver have the same size. But, this may not always be desirable. Furthermore, in many cases the critical issue is the power generated by, and the size of, the receiver, not the overall efficiency. Therefore, output power intensity, the ratio of output power to the receiver area, is another useful metric to consider.

The ratio of the size of receiver to the size of transmitter can also affect the efficiency. For example, if the transmitter is large, and the receiver is small, much of the acoustic energy transmitted may not be captured by the receiver. In this case, the efficiency will be low, but the power intensity at the receiver could still be high. Furthermore, this situation may address the application of medical devices quite well. Therefore, we define an area normalized efficiency, η', as shown in (33) where the standard definition of efficiency is modified by the transmitter area (A_{TX}) and receiver area (A_{RX}). This is equivalent to the ratio of output power intensity to input power intensity. Consider the case in which the area of a small receiver is held constant as the area of a larger transmitter is increased. If the transmit power intensity (P_{in}/A_{TX}) is constant, both the transmit area and input power will go up. However, received power will stay more or less constant. Efficiency, however, would go down. Thus, efficiency seems to unfairly penalize the small receiver. However, in this case, area normalized efficiency, η', would stay the same, which reflects the fact that the receiver has not changed. Thus η' is designed to address this shortcoming of efficiency as a metric when the transmitter is large and the receiver is small

$$\eta' = \frac{P_{out}}{P_{in}} \times \frac{A_{TX}}{A_{RX}} \times 100. \tag{33}$$

There are some cases in which the area normalized efficiency cannot be used properly unless several factors are taken in to account. If the transmitter diameter becomes too small compared to the wavelength, less energy will be captured by the receiver due to less radiation directivity. This can also cause the medium to reflect to the transmitter as a reactive load resulting in less radiated real power. Moreover, if the ratio of the diameter to the thickness is too small, then there would not be a pure vibration mode for the transmitter and the acoustic wave radiates in the medium in coupled modes which limits the efficiency. These issues are primarily features of relatively small transmitters. In that case, area normalized efficiency may not be an appropriate metric.

Table 4 provides a list of publications from the last 15 years including their important parameters. Only papers reporting experimental results are included in the table, and they are presented in the order of their publication year. The research team is identified by the first author on the corresponding paper. A few observations about these publications can be made.

The number of publications considering the diaphragm as the RX transducer are sparse compared to those considering the plate. Furthermore, none of them (with the exception of Christensen's work [28]) have compared the power generation potential of the plate and diaphragm when used as small, deeply implanted RX.

The vast majority of publications address, to some extent, the effect of RX depth on power generation. However, only a few of the publications take into consideration RX power sensitivity due to alignment and orientation. The papers that do address these effects present them in a narrow scope offering only experimental or simulation data for their particular device. This information is useful for the devices in question, but provides very little insight into other TX–RX systems. Mo, [92], provides the most information on alignment and orientation using FDTD simulations, but the analysis is still lacking in that it does not provide details about the effect that frequency and RX diameter have on RX power sensitivity.

Figure 14 plots the number of publications by year. It is clear that the number of publications for acoustic power transmission for implants has increased dramatically in recent years. Figure 15 shows the efficiency versus the area of the receiver for the reported devices with the best efficiency value of 50.4%. Larger receiver devices generally have higher efficiency. This may be because smaller receiver devices tend to have transmitters which are much larger than the receiver while for large devices the TX and RX are usually the same size. Thus small receiver devices are perhaps unfairly penalized by the efficiency metric. The area normalized efficiency

Table 4. Acoustic power transfer in implantable devices.

Article															
Author	Year/Ref	Transduction mechanism	Medium	Efficiency (%)	Input power (mW)	Output power (mW)	Operating frequency (kHz)	TX area (cm^2)	RX area (cm^2)	TX size (cm^3)	RX size (cm^3)	Depth (mm)	Power density (mW cm^{-3})	Power Intensity (mW cm^{-2})	η' (%)
Kawanabe	2001/[104]	PZT-plate	Goat Tissue	20	1700	340	1000	7.07	7.07	3.534	3.534		96.21	48.09	20
Suzuki	2002/[105]	PZT-plate	Skin	20	10 500	2100	1000	7.07	7.07	1.414	1.414	40	1485.15	297.03	20
Arra	2007/[56]	PZT-plate	Water	25	250	62.5	840	7.07	4.91	1.718	1.19	100	52.52	12.73	36
Lee	2007/[110]	PZT-diaphragm	Pork tissue	0.01	1.5	0.000 15	1.5		0.38		0.031	25	0.005	0.0004	
Shigeta	2009/[120]	PZT-plate	Water	0.35	229	0.8	4200	2.688	9.62	0.174	0.467	70	1.71	0.0832	0.098
Zhu	2010/[74]	Electrostatic	Air			2.14×10^{-5}	38.78					5			
Shih	2010/[111]	PZT-diaphragm	Pork tissue	0.015	1.23	0.000 18	35		0.38		0.031	60	0.0058	0.00047	
Ozeri	2010/[35]	PZT-plate	Pork tissue	27	260	70	673	1.77	1.77	0.53	0.53	5	132.1	39.55	27
Ozeri	2010/[36]	PZT-plate	Pork tTissue	39.1	256	100	650	1.77	1.77	0.53	0.53	5	188.67	56.50	39.1
Mazzilli	2010/[107]	PZT-plate	Water	10	30	3	1033	19.63	0.316			50		9.49	621.2
Shigeta	2011/[93]	PZT-plate	Water	50.4	20	10.08	1200	15.2	15.2	2.86	2.86	32.3	3.52	0.66	50.4
Larson	2011/[57]	PZT-plate	Rat hind limb	0.022	2300	0.51	1000	5.31	0.01		0.001	120	510	51	11.68
Maleki	2011/[46]	PZT-plate	Tissue			0.33	2150	52.4	0.05	5.345	0.0051	30	64.7	6.60	
Sanni	2012/[58]	PZT-plate	Water	1	800	8	200	0.78	0.78	0.078	0.078	70	102.56	10.26	1
Sanni	2013/[37]	PZT-plate	Water	0.2	488	0.976	200	0.78	0.78	0.078	0.078	80	12.51	1.25	0.2
Lee[a]	2013/[96]	PZT-plate	Pork tissue	21	15.5	3.25	255	19.63	19.63	15.7	15.7	23	0.21	0.17	21
Charthad	2014/[45], [121]	PZT-plate	Chicken breast			0.1	1000		0.01		0.0014	30	71.43	10	
Kim	2014/[106]	PZT-plate	Pork tissue	1.4×10^{-4}	11 700	0.016	0.35		0.4		0.0152	100	1.05	0.04	
He	2014/[88]	PZT-diaphragm	Pork tissue	0.096	51	0.049	40.43	23.76	0.1			22		0.49	22.81
Mazzilli	2014/[59]	PZT-plate	Water	1.6	1750	28	1000	21.3	0.3			105		93.33	113.6
Ozeri	2014/[70]	PZT-plate	Water			20	765	1.77	1.77	0.53	0.53	150	37.73	11.30	
Shmilovitz	2014/[122]	PZT-plate	Water			35	720	1.77	1.77	0.53	0.53	85	66.04	19.77	
Chou	2014/[99]	PZT-plate	Oil	1				0.15	0.15	0.046	0.046	25			1
Lee[a]	2014/[97]	PZT-platePZT-plate	Pork tissue	18	15.5	2.6	250	19.63	19.63	15.7	15.7	18	0.165	0.13	18
Song[a]	2015/[82]	PZT-plate	Water	0.15	7704	12	1150	10.7	0.08	2.14	0.016	200	750	150	20.06
Seo	2015/[66]	PZT-plate	Water				10 000					20			
Fang[a]	2015/[123]	PZT-plate	Pork tissue			3	3500		1.1		0.066	4		2.73	
Zhou	2015/[124], [125]	PZT-plate	Water				672		1.28		0.256	67			
Christensen[a]	2015/[28]	PZT-plate	Water	1.95	62.5	1.22	1058	1.29	1.29	0.24	0.24	40	5.08	0.94	1.95
		PZT-diaphragm	Water	0.016	62.5	0.001	3.5	1.29	0.5	0.24	0.005	40	0.2	0.002	0.041
Vihvelin[a]	2016/[126]	PZT-plate	Porcine tissue	25			1300	0.5	0.5	0.06	0.06	5			25

Table 4. (Continued.)

Article		Transduction mechanism	Medium	Efficiency (%)	Input power (mW)	Output power (mW)	Operating frequency (kHz)	TX area (cm^2)	RX area (cm^2)	TX size (cm^3)	RX size (cm^3)	Depth (mm)	Power density (mW cm^{-3})	Power Intensity (mW cm^{-2})	η' (%)
Author	Year/Ref														
Radziemski[a]	2016/ [127]	PZT-plate	Porcine tissue	22	2000	440	1000	4.91	4.91			5		89.61	22
Seo	2016/ [128]	PZT-plate		Tissue	0.12		1850		0.005			8.8			

[a] Best reported performance.

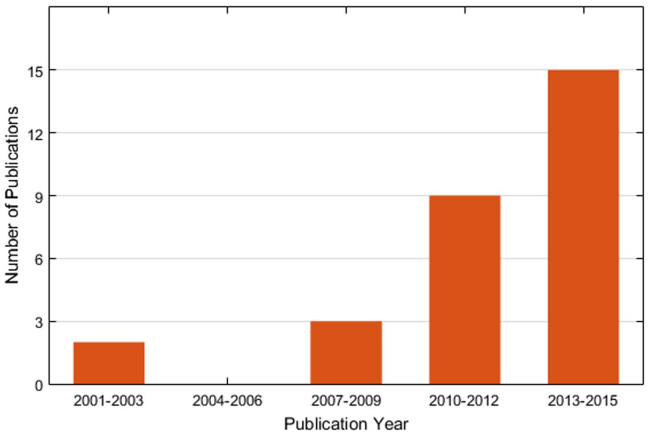

Figure 14. Number of publications of reported devices over the last 15 years.

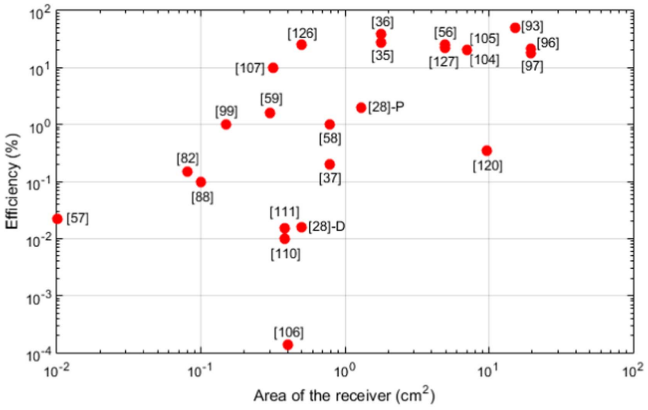

Figure 15. Efficiency versus area of the receiver for reported devices.

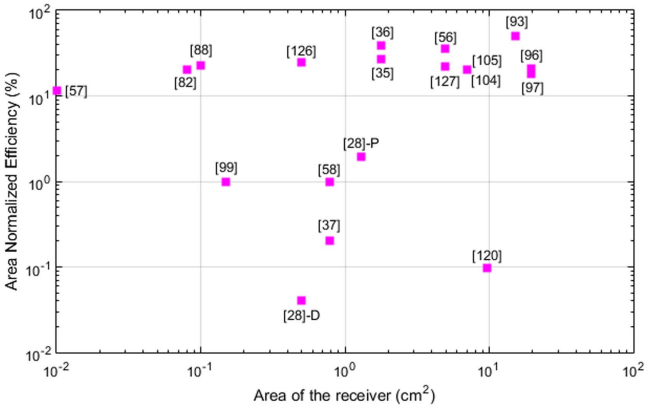

Figure 16. Area normalized efficiency versus area of the receiver for reported devices.

versus the receiver area is plotted in figure 16. It is clear that once normalizing for area, the trend of larger receivers exhibiting better efficiency goes away. One possible explanation is that the trend is due more to the size match of the transmitter and receiver rather than poor transduction performance on the part of the receiver. It should be noted that those devices with focused transducers are taken out from this figure since they result in area normalized efficiencies greater than 100%. Figure 17 shows the operating frequency of these

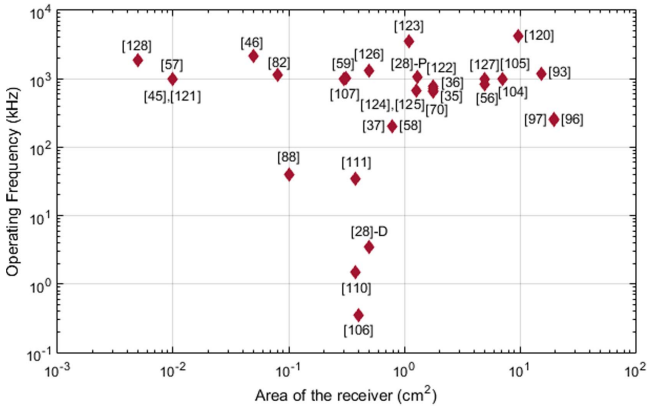

Figure 17. Operating frequency versus area of the receiver for reported device.

devices plotted against receiver size. The frequency values are mostly around 1 MHz. This is likely due to multiple factors which could include device size (half-wavelength thickness at 1 MHz is about 2 mm), and availability of commercial transducers operating at this frequency.

6. Conclusion

Implantable medical devices are now being widely used in order to monitor physiological parameters useful for medical diagnosis, provide therapeutic functions, and collect data for scientific studies. Although batteries have been used to power IMDs, they now consume a substantial portion of the device volume as the sizes of these devices have become smaller. Efforts to reduce overall implant size require focus on a suitable replacement for batteries, as battery technology has not kept pace with ever-shrinking modern electronics. Furthermore, batteries, having a fixed total energy, require replacement and, inevitably, surgery to carry out this replacement. Hence, further miniaturization, and therefore reduced trauma to the patient, will be greatly accelerated by the development of robust wireless powering techniques. Such wireless powering methods can miniaturize existing, and enable new real-time health monitoring and fuel more personalized and preventative healthcare. Common alternatives in the literature include RF, inductive coupling, vibrational energy harvesting, and APT.

APT is capable of obtaining more power with smaller devices compared to other methods. This is due to the fact that it has shorter wavelengths, which results in smaller sized receivers. Moreover, it exhibits lower attenuation in human tissue resulting in deeper penetration. This paper has covered the basic fundamentals of acoustic power transmission, discussed common modeling techniques, and reviewed the current state of the art as reported in the scientific literature. Modeling approaches can generally be broken down into analytical mathematical models, 1D lumped element models such as the Mason and KLM equivalent circuit models, and numerical finite element techniques. All methods are used in the scientific literature to provide design insight and

performance estimates. Analytical models have typically not dealt with issues of alignment or orientation. To fill the system modeling gap, there is still a need for a comprehensive design scheme that addresses a TX–RX system for differing architectures and diameters and considers power sensitivity due to depth, alignment, and orientation.

Reported implementations of APT for medical devices are showing progress on miniaturization. Among different transduction mechanisms, piezoelectric transduction seems to be more attractive since it can produce devices capable of generating higher power densities compared to electrostatic transduction. Although the piezoelectric plate structure can provide the required power for most implantable devices, a diaphragm structure may perform better for sub-mm size receivers especially implanted at large depths. Besides common metrics for comparing devices such as efficiency and power intensity, another performance figure of merit was defined and used in this paper for comparing APT for IMDs that is a function of device efficiency and also transmitter and receiver area. This area normalized efficiency does not appear to be a strong function of receiver size, indicating that very good acoustic power generation performance can be expected from very small devices.

Acknowledgment

The authors gratefully acknowledge funding for this work from the National Science Foundation under Award Number ECCS 1408265.

References

[1] Wood M A and Ellenbogen K A 2002 Cardiac pacemakers from the patient's perspective *Circulation* **105** 2136–8
[2] Ledet E H, D'Lima D, Westerhoff P, Szivek J A, Wachs R A and Bergmann G 2012 Implantable sensor technology: from research to clinical practice *J. Am. Acad. Orthop. Surg.* **20** 383–92
[3] Lueke J and Moussa W 2011 MEMS-based power generation techniques for implantable biosensing applications *Sensors* **11** 1433–60
[4] Gerrish P, Herrmann E, Tyler L and Walsh K 2005 Challenges and constraints in designing implantable medical ICs *IEEE Trans. Device Mater. Reliab.* **5** 435–44
[5] Guiseppi-Elie A, Brahim S, Slaughter G and Ward K 2005 Design of a subcutaneous implantable biochip for monitoring of glucose and lactate *IEEE Sens. J.* **5** 345–55
[6] Troyk P R, DeMichele G A, Kerns D A and Weir R F 2007 IMES: an implantable myoelectric sensor *Annual Int. Conf. IEEE Engineering in Medicine and Biology—Proc.* pp 1730–3
[7] Wise K D, Anderson D J, Hetke J F, Kipke D R and Najafi K 2004 Wireless implantable microsystems: high-density electronic interfaces to the nervous system *Proc. IEEE* **92** 76–97
[8] Zumsteg Z S, Kemere C, Member S, Driscoll S O, Member S, Santhanam G, Ahmed R E, Shenoy K V and Meng T H 2005 Power feasibility of implantable digital spike sorting circuits for neural prosthetic systems *IEEE Trans. Neural Syst. Rehabil. Eng.* **13** 272–9
[9] Owens B 1986 *Batteries for Implantable Biomedical Devices* (New York: Plenum)
[10] Bock D C, Marschilok A C, Takeuchi K J and Takeuchi E S 2012 Batteries used to power implantable biomedical devices *Electrochim. Acta* **84** 155–64
[11] Akhtar F and Rehmani M H 2015 Energy replenishment using renewable and traditional energy resources for sustainable wireless sensor networks: a review *Renew. Sustain. Energy Rev.* **45** 769–84
[12] Wei X and Liu J 2008 Power sources and electrical recharging strategies for implantable medical devices *Front. Energy Power Eng. China* **2** 1–13
[13] Rapoport B I, Kedzierski J T and Sarpeshkar R 2012 A glucose fuel cell for implantable brain–machine interfaces *PLoS One* **7** 1–15
[14] Kerzenmacher S, Ducrée J, Zengerle R and von Stetten F 2008 Energy harvesting by implantable abiotically catalyzed glucose fuel cells *J. Power Sources* **182** 1–17
[15] Roundy S and Wright P 2004 A piezoelectric vibration based generator for wireless electronics *Smart Mater. Struct.* **13** 1131–42
[16] Nasiri A, Zabalawi S A and Jeutter D C 2011 A linear permanent magnet generator for powering implanted electronic devices *IEEE Trans. Power Electron.* **26** 192–9
[17] Chen H, Liu M, Jia C and Wang Z 2009 Power harvesting using PZT ceramics embedded in orthopedic implants *IEEE Trans. Ultrason. Ferroelectr. Freq. Control* **56** 2010–4
[18] Karami M and Inman D 2012 Powering pacemakers from heartbeat vibrations using linear and nonlinear energy harvesters *Appl. Phys. Lett.* **100** 042901
[19] Karami M and Inman D 2011 Linear and nonlinear energy harvesters for powering pacemakers from heart beat vibrations *Proc. SPIE* **7977** 797703
[20] Hannan M A, Mutashar S, Samad S A and Hussain A 2014 Energy harvesting for the implantable biomedical devices: issues and challenges *Biomed. Eng. Online* **13** 79
[21] Cadei A, Dionisi A, Sardini E and Serpelloni M 2014 Kinetic and thermal energy harvesters for implantable medical devices and biomedical autonomous sensors *Meas. Sci. Technol.* **25** 12003
[22] Romero E, Warrington R O and Neuman M R 2009 Energy scavenging sources for biomedical sensors *Physiol. Meas.* **30** R35
[23] Ayazian S and Hassibi A 2011 Delivering optical power to subcutaneous implanted devices *2011 Annual Int. Conf. IEEE Engineering in Medicine and Biology Society* pp 2874–7
[24] Yang Y, Wei X-J and Liu J 2007 Suitability of a thermoelectric power generator for implantable medical electronic devices *J. Phys. D: Appl. Phys.* **40** 5790–800
[25] Ben Amar A, Kouki A B and Cao H 2015 Power approaches for implantable medical devices *Sensors* **15** 28889
[26] Kim A, Ochoa M, Rahimi R and Ziaie B 2015 New and emerging energy sources for implantable wireless microdevices *IEEE Access* **3** 89–98
[27] Paulo J and Gaspar P D 2010 Review and future trend of energy harvesting methods for portable medical devices *Proc. World Congress on Engineering* vol 2, pp 168–96
[28] Christensen D B and Roundy S 2015 Ultrasonically powered piezoelectric generators for bio-implantable sensors: plate versus diaphragm *J. Intell. Mater. Syst. Struct.* **27** 1092–105
[29] Denisov A and Yeatman E 2010 Ultrasonic versus inductive power delivery for miniature biomedical implants *2010 Int. Conf. on Body Sensor Networks* pp 84–9
[30] Shih Y, Shen T and Otis B 2011 A 2.3 W wireless intraocular pressure/temperature monitor *IEEE J. Solid-State Circuits* **46** 2592–601
[31] Ho J S, Yeh A J, Neofytou E, Kim S, Tanabe Y, Patlolla B, Beygui R E and Poon A S Y 2014 Wireless power transfer

to deep-tissue microimplants *Proc. Natl Acad. Sci. USA* **111** 7974–9
[32] O'driscoll S, Poon A and Meng T 2014 Wireless power transmission for implantable medical devices *US Patent* 8,634,928
[33] Waffenschmidt E and Staring T 2009 Limitation of inductive power transfer for consumer applications *13th European Conference on Power Electronics and Applications, 2009. EPE '09* pp 1–10
[34] Roes M G, Duarte J L, Hendrix M A and Lomonova E A 2013 Acoustic energy transfer: a review *IEEE Trans. Ind. Electron.* **60** 242–8
[35] Ozeri S and Shmilovitz D 2010 Ultrasonic transcutaneous energy transfer for powering implanted devices *Ultrasonics* **50** 556–66
[36] Ozeri S, Shmilovitz D, Singer S and Wang C C 2010 Ultrasonic transcutaneous energy transfer using a continuous wave 650 kHz Gaussian shaded transmitter *Ultrasonics* **50** 666–74
[37] Sanni A and Vilches A 2013 Powering low-power implants using PZT transducer discs operated in the radial mode *Smart Mater. Struct.* **22** 115005
[38] Lu X, Wang P and Niyato D 2015 Wireless networks with RF energy harvesting: a contemporary survey *IEEE Commun. Surv. Tutorials* **17** 757–89
[39] Lu X, Wang P, Niyato D, Kim D I and Han Z 2015 Wireless charging technologies: fundamentals, standards, and network applications *IEEE Commun. Surv. Tutorials* **18** 1413–52
[40] Shinohara N 2011 Power without wires *IEEE Microw. Mag.* **12** S64–73
[41] Walleczek J 1992 Electromagnetic field effects on cells of the immune system: the role of calcium signaling *FASEB J.* **6** 3177–85
[42] Meral I, Mert H, Mert N, Deger Y and Yoruk I 2007 Effects of 900 MHz electromagnetic field emitted from cellular phone on brain oxidative stress and some vitamin levels of guinea pigs *Brain Res.* **1169** 120–4
[43] Liao Y, Yao H, Lingley A, Parviz B and Otis B P 2012 A 3-CMOS glucose sensor for wireless contact-lens tear glucose monitoring *IEEE J. Solid-State Circuits* **47** 335–44
[44] Van Schuylenbergh K and Puers R 2009 *Inductive Powering: Basic Theory and Application to Biomedical Systems* (Netherlands: Springer)
[45] Charthad J, Weber M J, Chang T C and Arbabian A 2015 A mm-sized implantable medical device (IMD) with ultrasonic power transfer and a hybrid Bi-directional data link *IEEE J. Solid-State Circuits* **50** 1741–53
[46] Maleki T, Cao N, Hyun Song S, Kao C, Chu S, Ko A and Ziaie B 2011 An ultrasonically powered implantable micro-oxygen generator (IMOG) *IEEE Trans. Biomed. Eng.* **58** 3104–11
[47] Poon A, O'Driscoll S and Meng T 2010 Optimal frequency for wireless power transmission into dispersive tissue *IEEE Trans. Antennas Propag.* **58** 1739–50
[48] Food and Drug Administration 2008 'Guidance for Industry and FDA—Staff Information for Manufacturers Seeking Marketing Clearance of Diagnostic Ultrasound Systems and Transducers' Silver Spring US FDA
[49] O'Driscoll S, Poon A and Meng T H 2009 A mm-sized implantable power receiver with adaptive link compensation *2009 IEEE Int. Solid-State Circuits Conf.—Digest of Technical Papers* (doi:10.1109/ISSCC.2009.4977424)
[50] Jow U and Ghovanloo M 2007 Design and optimization of printed spiral coils for efficient transcutaneous inductive power transmission *IEEE Trans. Biomed. Circuits Syst.* **1** 193–202
[51] Kilinc E, Dehollain C and Maloberti F 2010 Design and optimization of inductive power transmission for implantable sensor system *Proc. SM2ACD'10* (doi:10.1109/SM2ACD.2010.5672335)
[52] Kiani M and Ghovanloo M 2010 An RFID-based closed-loop wireless power transmission system for biomedical applications *IEEE Trans. Circuits Syst.* II **57** 260–4
[53] Kiani M, Kwon K and Zhang F 2011 Evaluation of a closed loop inductive power transmission system on an awake behaving animal subject *2011 Annual Int. Conf. of the IEEE Engineering in Medicine and Biology Society* (Piscataway, NJ: IEEE) (doi:10.1109/IEMBS.2011.6091887)
[54] Silay K, Dehollain C and Declercq M 2011 Inductive power link for a wireless cortical implant with two-body packaging *IEEE Sens. J.* **11** 2825–33
[55] Liu X, Berger J, Ogirala A and Mickle M H 2013 A touch probe method of operating an implantable RFID tag for orthopedic implant identification *IEEE Trans. Biomed. Circuits Syst.* **7** 236–42
[56] Arra S, Leskinen J, Heikkilä J and Vanhala J 2007 Ultrasonic power and data link for wireless implantable applications *2007 2nd Int. Symp. Wireless Pervasive Computing* (doi:10.1109/ISWPC.2007.342668)
[57] Larson P J and Towe B C 2011 Miniature ultrasonically powered wireless nerve cuff stimulator *2011 5th Int. IEEE/EMBS Conf. on Neural Engineering (NER)* (Piscataway, NJ: IEEE) (doi:10.1109/NER.2011.5910538)
[58] Sanni A, Vilches A and Toumazou C 2012 Inductive and ultrasonic multi-tier interface for low-power, deeply implantable medical devices *IEEE Trans. Biomed. Circuits Syst.* **6** 297–308
[59] Mazzilli F, Lafon C and Dehollain C 2014 A 10.5 cm ultrasound link for deep implanted medical devices *IEEE Trans. Biomed. Circuits Syst.* **8** 738–50
[60] Briand D, Yeatman E and Roundy S (ed) 2015 *Micro Energy Harvesting* (Weinheim: Wiley)
[61] Kinsler L and Frey A 2000 *Fundamentals of Acoustics* 4th edn (New York: Wiley)
[62] Nakamura K 2012 *Ultrasonic Transducers: Materials and Design for Sensors, Actuators and Medical Applications* (Amsterdam: Elsevier)
[63] Hu Y C, Liao P L, Shih W P, Wang X Y and Chang P Z 2009 Study on the acoustic impedance matching of human tissue for power transmitting/charging system of implanted biochip *2009 IEEE 3rd Int. Conf. on Nano/Molecular Medicine and Engineering, NANOMED 2009* (doi:10.1109/NANOMED.2009.5559087)
[64] Zaid T, Saat S, Yusop Y and Jamal N 2014 Contactless energy transfer using acoustic approach—a review *2014 Int. Conf. on. IEEE Computer, Communications, and Control Technology (I4CT)* (doi:10.1109/I4CT.2014.6914209)
[65] Seo D, Carmena J M, Rabaey J M, Alon E and Maharbiz M M 2013 Neural dust: an ultrasonic, low power solution for chronic brain–machine interfaces arXiv:1307.2196
[66] Seo D, Carmena J M, Rabaey J M, Maharbiz M M and Alon E 2015 Model validation of untethered, ultrasonic neural dust motes for cortical recording *J. Neurosci. Methods* **244** 114–22
[67] Inoue T, Ohta M and Takahashi S 1987 Design of ultrasonic transducers with multiple acoustic matching layers for medical application *IEEE Trans. Ultrason. Ferroelectr. Freq. Control* **34** 8–16
[68] Hill R and El-Dardiry S 1980 A theory for optimization in the use of acoustic emission transducers *J. Acoust. Soc. Am.* **67** 673–82
[69] Callens D, Bruneel C and Assaad J 2004 Matching ultrasonic transducer using two matching layers where one of them is glue *NDT E Int.* **37** 591–6
[70] Ozeri S and Shmilovitz D 2014 Simultaneous backward data transmission and power harvesting in an ultrasonic

transcutaneous energy transfer link employing acoustically dependent electric impedance modulation *Ultrasonics* **54** 1929–37
[71] American Institute of Ultrasound in Medicine and National Electrical Manufacturers Association 1998 *Acoustic Output Measurement Standard for Diagnostic Ultrasound Equipment* (Laurel, MD: American Institute of Ultrasound in Medicine)
[72] Culjat M O, Goldenberg D, Tewari P and Singh R S 2010 A review of tissue substitutes for ultrasound imaging *Ultrasound Med. Biol.* **36** 861–73
[73] Narayana P, Ophir J and Maklad N 1984 The attenuation of ultrasound in biological fluids *J. Acoust. Soc. Am.* **76** 1–4
[74] Zhu Y, Moheimani S O R and Yuce M R 2010 Ultrasonic energy transmission and conversion using a 2D MEMS resonator *IEEE Electron Device Lett.* **31** 374–6
[75] Banerji S, Goh W, Cheong J H and Je M 2013 CMUT ultrasonic power link front-end for wireless power transfer deep in body *2013 IEEE MTT-S Int. Microwave Workshop Series on RF and Wireless Technologies for Biomedical and Healthcare Applications (IMWS-BIO)* (doi:10.1109/IMWS-BIO.2013.6756176)
[76] Chen S N, Wang G J and Chien M C 2006 Analytical modeling of piezoelectric vibration-induced micro power generator *Mechatronics* **16** 379–87
[77] Aktakka E E, Peterson R L and Najafi K 2013 Wafer-level integration of high-quality bulk piezoelectric ceramics on silicon *IEEE Trans. Electron Devices* **60** 2022–30
[78] Leach W M 1994 Controlled-source analogous circuits and SPICE models for piezoelectric transducers *IEEE Trans. Ultrason. Ferroelectr. Freq. Control* **41** 60–6
[79] Krimholtz R, Leedom D A and Matthaei G L 1970 New equivalent circuits for elementary piezoelectric transducers *Electron. Lett.* **13** 398–9
[80] Mason W 1948 *Electromechanical Transducers and Wave Filters* (New York, Van Nostrand)
[81] Sherrit S, Leary S P, Dolgin B P and Bar-Cohen Y 1999 Comparison of the Mason and KLM equivalent circuits for piezoelectric resonators in the thickness mode *1999 Proc. Ultrasonics Symp.* vol 2 (doi:10.1109/ULTSYM.1999.849139)
[82] Song S H, Kim A and Ziaie B 2015 Omni-directional ultrasonic powering for mm-scale implantable biomedical devices *IEEE Trans. Biomed. Eng.* **62** 2717–23
[83] Redwood M 1961 Transient performance of a piezoelectric transducer *J. Acoust. Soc. Am.* **33** 527–36
[84] Ensminger D and Bond L 2011 *Ultrasonics: Fundamentals, Technologies, and Applications* (Boca Raton, FL: CRC)
[85] Shahab S, Gray M and Erturk A 2015 An experimentally validated contactless acoustic energy transfer model with resistive-reactive electrical loading *Proc. SPIE* **9431** 943105
[86] Shahab S, Gray M and Erturk A 2015 Ultrasonic power transfer from a spherical acoustic wave source to a free–free piezoelectric receiver: modeling and experiment *J. Appl. Phys.* **117** 104903
[87] Hori Y, Fujimori K, Tsuruta K and Nogi S 2013 Design and development of highly efficient transducer for ultrasonic wireless power transmission system *IEEE J. Trans. Electron. Inf. Syst.* **184** 337–43
[88] He Q, Liu J, Yang B, Wang X, Chen X and Yang C 2014 MEMS-based ultrasonic transducer as the receiver for wireless power supply of the implantable microdevices *Sensors Actuators* A **219** 65–72
[89] Treeby B and Cox B 2010 *k*-wave: MATLAB toolbox for the simulation and reconstruction of photoacoustic wave fields *J. Biomed. Opt.* **15** 021314
[90] Fowler A, Moheimani S O R and Behrens S 2014 An omnidirectional MEMS ultrasonic energy harvester for implanted devices *J. Microelectromech. Syst.* **23** 1454–62
[91] Hallaj I and Cleveland R 1999 FDTD simulation of finite-amplitude pressure and temperature fields for biomedical ultrasound *J. Acoust. Soc. Am.* **105** L7–12
[92] Mo C, Hudson S and Radziemski L J 2013 Effect of misalignment between ultrasound piezoelectric transducers on transcutaneous energy transfer *Proc. SPIE* **8688** 868814
[93] Shigeta Y and Hori Y 2011 Development of highly efficient transducer for wireless power transmission system by ultrasonic *2011 IEEE MTT-S Int. Microwave Workshop Series on Innovative Wireless Power Transmission: Technologies, Systems, and Applications (IMWS)* (doi:10.1109/IMWS.2011.5877115)
[94] Shaul O, Boaz S and Doron S 2012 Non-invasive sensing of the electrical energy harvested by medical implants powered by an ultrasonic transcutaneous energy transfer link *2012 IEEE Int. Symp. on Industrial Electronics (ISIE)* (doi:10.1109/ISIE.2012.6237251)
[95] Fowler A, Moheimani S O R and Behrens S 2013 A 3-DOF SOI MEMS ultrasonic energy harvester for implanted devices *J. Phys.: Conf. Ser.* **476** 012002
[96] Lee S Q, Youm W and Hwang G 2013 Biocompatible wireless power transferring based on ultrasonic resonance devices *Proc. Meet. Acoust.* **19** 030030
[97] Lee S, Youm W, Hwang G, Moon K S and Ozturks Y 2014 Resonant ultrasonic wireless power transmission for bio-implants *Proc. SPIE* **9057** 90570J
[98] Shahab S and Erturk A 2014 Contactless ultrasonic energy transfer for wireless systems: acoustic-piezoelectric structure interaction modeling and performance enhancement *Smart Mater. Struct.* **23** 125032
[99] Chou T, Subramanian R, Park J and Mercier P 2014 A miniaturized ultrasonic power delivery system *2014 IEEE Biomedical Circuits and Systems Conf. (BioCAS) Proc.* (doi:10.1109/BioCAS.2014.6981757)
[100] Fowler A G and Moheimani S O R 2015 4-DOF SOI-MEMS ultrasonic energy harvester *2015 IEEE 15th Int. Conf. on Nanotechnology (IEEE-NANO)* (doi:10.1109/NANO.2015.7388922)
[101] Roundy S, Wright P K and Pister K S J 2002 Micro-electric vibration-to-electricity converters *ASME 2002 Int. Mechanical Engineering Congress and Exposition* (American Society of Mechanical Engineers) (doi:10.1115/IMECE2002-39309)
[102] Zhu Y, Moheimani S O R and Yuce M R 2011 A 2-DOF MEMS ultrasonic energy harvester *IEEE Sens. J.* **11** 155–61
[103] Zhu Y, Moheimani S O R and Yuce M R 2009 A 2-DOF wideband electrostatic transducer for energy harvesting and implantable applications *2009 IEEE Sensors* (doi:10.1109/ICSENS.2009.5398476)
[104] Kawanabe H, Katane T, Saotome H, Saito O and Kobayashi K 2001 Power and information transmission to implanted medical device using ultrasonic *Japan J. Appl. Phys.* **40** 3865
[105] Suzuki S-N, Kimura S, Katane T, Saotome H, Saito O and Kobayashi K 2002 Power and interactive information transmission to implanted medical device using ultrasonic *Japan J. Appl. Phys.* **41** 3600
[106] Kim A, Powell C R and Ziaie B 2014 An implantable pressure sensing system with electromechanical interrogation scheme *IEEE Trans. Biomed. Eng.* **61** 2209–17
[107] Mazzilli F, Peisino M, Mitouassiwou R, Cotte B, Thoppay P, Lafon C, Favre P, Meurville E and Dehollain C 2010 In-vitro platform to study ultrasound as source for wireless energy transfer and communication for implanted medical devices *2010 Annual Int. Conf. of the IEEE Engineering in Medicine and Biology* (doi:10.1109/IEMBS.2010.5627541)
[108] Duck F, Baker A and Starritt H 1998 *Ultrasound in Medicine* (Boca Raton, FL: CRC Press)

[109] Dogheche K, Cavallier B, Delobelle P, Hirsinger L, Cattan E, Rèmiens D, Marzencki M, Charlot B, Basrour S and Ballandras S 2006 A Bi-Stable micro-machined piezoelectric transducer for mechanical to electrical energy transformation *Integr. Ferroelectr.* **76** 3–12

[110] Lee B-S, Shih P-J, He J-J, Shih W-P and Wu W-J 2007 A study of implantable power harvesting transducers *Proc. SPIE* **6530** 65300I

[111] Shih P J and Shih W P 2010 Design, fabrication, and application of bio-implantable acoustic power transmission *J. Microelectromech. Syst.* **19** 494–502

[112] Shih P-J, Weng W-P, Shih W-P, Tsai Y-C and Chang P-Z 2007 Acoustic polarization for optimized implantable power transimittion *2007 IEEE 20th Int. Conf. on Micro Electro Mechanical Systems MEMS.* (doi:10.1109/MEMSYS.2007.4433136)

[113] Pardo R L J, García A, Brebøl K, Leighton G and Huang Z 2010 Impedance measurements for determination of elastic and piezoelectric coefficients of films *Adv. Appl. Ceram.* **109** 156–61

[114] Kanno I, Fujii S, Kamada T and Takayama R 1997 Piezoelectric properties of *c*-axis oriented Pb(Zr, Ti)O_3 thin film *Appl. Phys. Lett.* **70** 1378–80

[115] Hindrichsen C G, Lou-Moller R, Hansen K and Thomsen E V 2010 Advantages of PZT thick film for MEMS sensors *Sensors Actuators* A **163** 9–14

[116] Vrejoiu B I, Le Rhun G, Pintilie L, Hesse D and Alexe M 2006 Intrinsic ferroelectric properties of strained tetragonal PbZr0. 2Ti0. 8O3 obtained on layer-by-layer grown, defect-free single-crystalline films *Adv. Mater.* **18** 1657–61

[117] Aktakka E E, Kim H and Najafi K 2009 Wafer level fabrication of high performance MEMS using bonded and thinned bulk piezoelectric substrates *TRANSDUCERS 2009—2009 Int. Solid-State Sensors, Actuators and Microsystems Conf.* (doi:10.1109/SENSOR.2009.5285795)

[118] Aktakka E E and Najafi K 2015 Three-axis piezoelectric vibration energy harvester *2015 28th IEEE Int. Conf. on Micro Electro Mechanical Systems (MEMS)* (doi:10.1109/MEMSYS.2015.7051166)

[119] Tang G *et al* 2012 Fabrication and analysis of high-performance piezoelectric MEMS generators *J. Micromech. Microeng.* **22** 65017

[120] Shigeta Y, Yamamoto T, Fujimori K, Sanagi M, Nogi S and Tsukagoshi T 2009 Development of ultrasonic wireless power transmission system for implantable electronic devices *2009 European Wireless Technology Conf. (EuWIT 2009)* (Piscataway, NJ: IEEE)

[121] Charthad J, Weber M J, Chang T C, Saadat M and Arbabian A 2014 A mm-sized implantable device with ultrasonic energy transfer and RF data uplink for high-power applications *Proc. IEEE 2014 Custom Integrated Circuits Conf.* (doi:10.1109/CICC.2014.6946071)

[122] Shmilovitz D, Ozeri S, Wang C-C and Spivak B 2014 Noninvasive control of the power transferred to an implanted device by an ultrasonic transcutaneous energy transfer link *IEEE Trans. Biomed. Eng.* **61** 995–1004

[123] Fang B, Feng T, Zhang M and Chakrabartty S 2015 Feasibility of B-mode diagnostic ultrasonic energy transfer and telemetry to a cm 2 sized deep-tissue implant *2015 IEEE Int. Symp. on Circuits and Systems (ISCAS)* (doi:10.1109/ISCAS.2015.7168750)

[124] Zhou J, Kim A, Song S H and Ziaie B 2015 An ultrasonically powered implantable micro-light source for localized photodynamic therapy *Transducers-2015 18th Int. Conf. Solid-State Sensors, Actuators Microsystems, (TRANSDUCERS 2015)* pp 876–9

[125] Zhou J, Kim A and Ziaie B 2015 An ultrasonically controlled power management system for implantable biomedical devices *Biomedical Circuits and Systems Conf. (BioCAS)* (doi:10.1109/BioCAS.2015.7348297)

[126] Vihvelin H, Leadbetter J, Bance M, Brown J A and Adamson R B A 2016 Compensating for tissue changes in an ultrasonic power link for implanted medical devices *IEEE Trans. Biomed. Circuits Syst.* **10** 404–11

[127] Radziemski L and Makin I R S 2016 *In vivo* demonstration of ultrasound power delivery to charge implanted medical devices via acute and survival porcine studies *Ultrasonics* **64** 1–9

[128] Seo D, Neely R M, Shen K, Rabaey J M, Carmena J M, Maharbiz M M, Singhal U and Alon E 2016 Wireless recording in the peripheral nervous system with ultrasonic neural dust neuron neuroresource wireless recording in the peripheral nervous system with ultrasonic neural dust *Neuron* **91** 1–11